LP2SS

Efficient conversion of lamination parameters into stacking sequences using fast Fourier transforms and branch & bound

Manikandan, Rakshith; Peeters, D. M.J.; van Campen, J. M.J.F.; Dähne, Sascha; Zerbst, David; Hühne, Christian

Important note
To cite this publication, please use the final published version (if applicable).
Please check the document version above.

LP2SS: Efficient conversion of lamination parameters into stacking sequences using fast Fourier transforms and branch & bound

Rakshith Manikandan [a,b],*, D.M.J. Peeters [b], J.M.J.F. van Campen [b], Sascha Dähne [a], David Zerbst [a], Christian Hühne [a]

[a] German Aerospace Center (DLR), Institute of Lightweight Systems, Lilienthalplatz 7, Braunschweig, 38108, Germany
[b] Department of Aerospace Structures & Materials, Faculty of Aerospace Engineering, Delft University of Technology (TU Delft), Kluyverweg 1, Delft, 2629 HS, The Netherlands

ARTICLE INFO

ABSTRACT

Fibre-reinforced laminated composites are constructed layer-by-layer, enabling ease of directional stiffness tailoring. Their vast design space is typically explored using two-steps. First, the optimum stiffness for given loads is conceptualised using continuous optimisation of lamination parameters (LPs). Then, discrete optimisation determines a fibre stacking sequence (SS) that closely matches these LPs. While fibre angles are conventionally limited to 45° multiples, finer increments (e.g., ±15°) can enable lighter structures. However, existing SS design methods do not scale well with this increased problem dimensionality. To overcome this challenge, we propose LP2SS, a novel methodology utilising fast Fourier transforms (FFT) and a branch-and-bound optimiser. By treating LPs as a signal, FFTs identify the number of fibre layers oriented at different angles, akin to estimating the magnitude of different frequencies within a signal. This fibre angle distribution guides the branch-and-bound optimiser, enabling efficient SS design with accurate LP matching, while satisfying empirical design rules. The ingenious use of FFTs is key to LP2SS's performance, achieving solutions within tenths of a second, compared to minutes required by state-of-the-art methods. Validated on established benchmarks and a newly proposed comprehensive test set, LP2SS marks a significant advancement in the optimal design of large-scale laminated composite structures.

1. Introduction

As demand for commercial aviation rises, governments have set ambitious emission reduction goals [1]. One approach to achieve this is to enhance fuel economy by reducing structural weight. Fibre-reinforced laminated composites have been essential in this effort, owing to superior specific strength relative to their isotropic counterparts (metallic alloys). Today, they comprise over half the structural weight of modern aircraft [2,3]. Meanwhile, researchers are working on further weight reduction by capitalising on their layer-by-layer construction and tailoring directional stiffness throughout a structure [4,5].

From an optimisation perspective, the design variables of laminated composites (ply[1] thickness and fibre orientation in each of N layers) belong to a discrete set of allowable values. This results in a vast, discrete, and non-convex design space, posing a complex optimisation problem [6–8]. For circumventing this, a two-step design procedure is commonly followed, among other multi-step variants [9]. First,

the composite's conceptual stiffness is optimised for given loads with lamination parameters (LPs). Then, a stacking sequence (SS) of different plies is designed to match the optimum stiffness. Commonly, LPs are designed using continuous optimisation, while SS is designed to match the LPs using discrete optimisation [6]. This separation helps manage the problem's inherent complexity.

Historically, engineers opted to orient fibres only along multiples of 45° ($\theta \in [0, \pm45, 90]$) (or [$\Delta45°$]), for analytical and manufacturing convenience [10]. Such laminates still remain prevalent, owing to years of experience making aircraft with them. However, more weight reduction can be enabled with a broader range of angles like $\theta \in [0, \pm15, \pm30, \pm45, \pm60, \pm75, 90]$ (or [$\Delta15°$]), as the fibre's directional properties are better utilised [5]. At the same time, structural design is largely governed by response-driven constraints (e.g., strain failure/buckling), and SS design guidelines (e.g., Symmetry, Balance, 10% Rule, Disorientation, etc.) to eliminate unwanted stiffness coupling and be robust under in-service loads [11,12]. As such, expanding the

---

number of allowable fibre angles increases design options, but also magnifies the computational challenge.

Although genetic algorithms [13] and branch & bound [14] are widely used for SS design, benchmark studies show nearly a four-fold increase in their computation time when expanding fibre angle choices from $[\Delta 45°]$ to $[\Delta 15°]$ [14]. In response, this paper presents a robust and efficient SS design method, to match conceptual stiffness described by given LPs. The following section review existing approaches and highlight the need for improved methods to design SS with $[\Delta 15°]$.

2. Preliminaries: Design and optimisation using lamination parameters

The design space offered by laminated composites can be effectively navigated, as described in Fig. 1. First, the conceptual optimum stiffness is determined using LPs, and then the SS is designed to match that optimal stiffness.
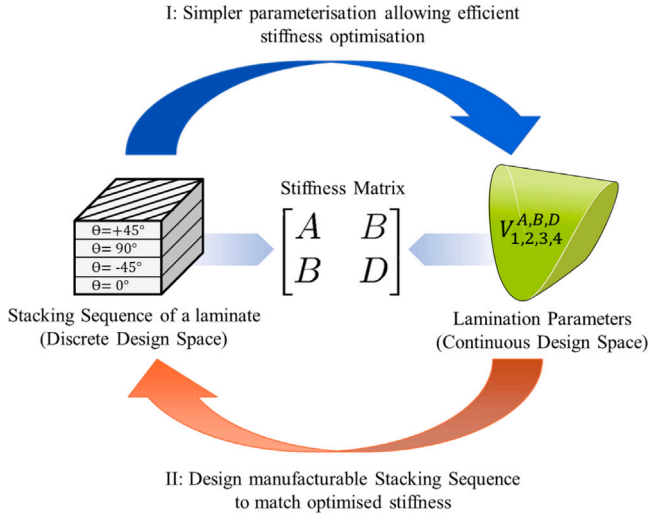

Fig. 1. Overview of Laminate Design using LPs.

For completeness, it is noted that, to the best of the authors' knowledge, LP-based designs are not yet used in the aerospace industry. A brief overview of the industry's current design practices is provided in Appendix A.1.

Classical laminated plate theory describes laminate stiffness using the ABD matrix: A- Extensional Stiffness, B- Coupling Stiffness, and D- Flexural Stiffness. In order to determine the conceptual optimum stiffness, the directional stiffness values in the matrix can be optimised. However, given that these values are highly correlated, assigning them arbitrarily is challenging. Hence, Tsai et al. [15] parameterised laminate material properties using trigonometric identities to linearly describe ABD using laminate height h and 12 non-dimensional quantities (the LPs)[2].

$$
\begin{aligned}
A &= h(\Gamma_0 + \Gamma_1 V_1^A + \Gamma_2 V_2^A + \Gamma_3 V_3^A + \Gamma_4 V_4^A) \\
B &= \frac{h^2}{4}(\Gamma_1 V_1^B + \Gamma_2 V_2^B + \Gamma_3 V_3^B + \Gamma_4 V_4^B) \quad (1)\\
D &= \frac{h^3}{12}(\Gamma_0 + \Gamma_1 V_1^D + \Gamma_2 V_2^D + \Gamma_3 V_3^D + \Gamma_4 V_4^D)
\end{aligned}
$$

Here, $V_{[1,2,3,4]}^{\{A,B,D\}}$ are the 12 LPs, and Γ entities are matrices describing ply material properties that are invariant to orientation (see Appendix A.2 for formulations). For Symmetric-Balanced laminates, 6 LPs (V^B and $V_{3,4}^A$) can be nullified in optimisation. Mathematically, the LPs

---

[2] LPs are valid only for the design of laminates or sandwich structures [16], with plies and/or core, respectively, made of the same material.

form a continuous and convex design space [17], making the use of gradient-based optimisation particularly effective. While each LP can numerically lie within $[-1, 1]$, the design domain is not a full 12D hypercube due to inherent correlations among them [10]. Appendix A.3 gives an overview of how design space and constraints can be defined for LP optimisation.

SS design is now performed such that their LPs closely match the conceptual optimum from the previous step. For a given SS with equi-thickness plies, its LPs are calculated as follows:

$$
\begin{aligned}
V_{[1,2,3,4]}^A &= \frac{1}{N} \sum_{k=1}^{N} [\cos 2\theta_k, \cos 4\theta_k, \sin 2\theta_k, \sin 4\theta_k] \\
V_{[1,2,3,4]}^B &= \frac{2}{N^2} \sum_{k=1}^{N} \left\{ \left(\frac{N}{2} - k + 1\right)^2 - \left(\frac{N}{2} - k\right)^2 \right\} [\cos 2\theta_k, \cos 4\theta_k, \sin 2\theta_k, \sin 4\theta_k] \quad (2)\\
V_{[1,2,3,4]}^D &= \frac{4}{N^3} \sum_{k=1}^{N} \left\{ \left(\frac{N}{2} - k + 1\right)^3 - \left(\frac{N}{2} - k\right)^3 \right\} [\cos 2\theta_k, \cos 4\theta_k, \sin 2\theta_k, \sin 4\theta_k]
\end{aligned}
$$

Here, θ_k represents the orientation of the kth ply. Now, the task is to design a discrete SS whose LPs match the optimised set. These SS also need to satisfy empirical design guidelines that are commonly followed in the aerospace industry [12,18,19]:

1. To nullify in-plane and out-plane coupling stiffness (B matrix), mid-plane **symmetry** of a stacking sequence can be enforced. Eliminating this behaviour without symmetry is explored by York et al. [20].

2. To nullify coupling responses within the A matrix (extension-shear coupling), the off-axis plies (orientations apart from 0 and 90) can occur in **balanced** pairs, that is, every $+\theta$ should have a $-\theta$. Such in-plane orthotropy can also be achieved without the balancing rule [21].

3. The **10% Rule** requires at least 10% of plies to be oriented along the four principal directions (0, ±45, 90°), ensuring minimum in-plane stiffness for protection under secondary loads. For non-conventional orientations ($[\Delta 15°]$), a more generalised version [19,22] ensures adequate stiffness across all directions.

4. To induce less residual stresses in the laminate while curing, the **disorientation** guideline restricts orientation change between consecutive layers not to exceed 45°.

5. To avoid crack bridging, the **contiguity** guideline does not allow more than 0.6 mm of material with the same orientation to be placed together.

6. For **damage tolerance** against impact and improved buckling performance, surface layers should have a ±45° ply.

Designing an N-layer SS (discrete) while matching the optimum LPs (continuous) and satisfying these design guidelines can be a complex computational task. The jump between these two design spaces — converting LPs, i.e., predetermined stiffnesses, into an SS — is commonly referred to as the 'inverse problem' of laminate design. Over the past few decades, many solutions have been proposed to address this challenge [6,23]. They can be broadly classified into five categories: Analytical, Gradient-based, Mixed-Integer Linear Programming, Population-based, and Layerwise approaches.

Analytical Methods: Miki [24] proposed a simple formulation to design a Symmetric-Balanced SS with up to three orientations [$\pm\theta_1, \pm\theta_2$, $\theta_3 = 0°$], matching only V^A LPs, with user-defined ply fraction. Hammer [25] showed that a three-layer SS is enough to match any set of V^A LPs, while Autio [26] showed a two-layer SS sufficed for any set of V^D LPs. With conventional angles ($[\Delta 45°]$), Diaconu [27] considered both V^A and V^D LPs together. However, these techniques treat ply thickness as a continuous variable—making them impractical. Van Campen et al. [28] proposed a practical solution for analytically designing a four-layer Symmetric-Balanced SS ($[\pm\theta_1, \pm\theta_2]_S$). Viquerat et al. [29] then accessed a broader design space by designing more than four layers of an SS ($[\pm\theta_1, \pm\theta_2, \ldots, \pm\theta_{N/2}]_S$) using polynomial homotopy continuation (PHC). This method can solve a system of equations,

Table 1

Comparison of state-of-the-art SS Design methods from LPs using [Δ45°], and their overall performance scalability to [Δ15°] designs.

	Guideline enforcement	Design Space Exploration	Solution Quality	Computational Efficiency	Performance Scalability for [Δ15°]
Analytical	+	−	−	+	−
Gradient	+	−	−	−	−
Population	+	+	−	−	−
Layerwise	+	+	+	+	−
MILP	−	−	−	+	−

even with more unknown values than equations (non-square systems). Nevertheless, PHC is sensitive to initial parameters and computationally expensive: approximately two hours to solve square systems (e.g., a 12-layer SS to match 12 LPs), with non-square cases taking longer.

Gradient-based Methods: By using local gradient information, the angles within an N-layer SS can be iteratively optimised to minimise the mismatch between target and realised LPs. Grédiac used the steepest-descent method with a least-squares objective [30,31], while Peeters et al. [32] applied the method of moving asymptotes with a convex-quadratic approximation of structural responses. Given the discrete and non-convex nature of the problem, these techniques often struggle to escape local minima as the dimensionality increases. Sankalp et al. [33] introduced deflation constraints to address this, though their computational performance remains untested.

Mixed-Integer Linear Programming: Non-gradient-based approaches, such as Mixed-Integer Linear Programming (MILP), enable handling constrained optimisation tasks with both discrete and continuous design variables. They have been used for SS design in various studies [34,35], with recent implementations by Ntourmas et al. [36] demonstrating effectiveness even for variable stiffness designs from LPs. These methods require explicit formulation of design guidelines as constraints, and their scalability with increasing problem size remains uncertain. More recently, a novel study re-cast the MILP formulation using quantum computing operators [37] (density matrix renormalisation group algorithm, or DMRG), showing competitive computational efficiency on the order of a few minutes for SS design with [Δ45°] plies while enforcing design guidelines using penalties [38]. However, DMRG is nondeterministic and its scalability with [Δ15°] angles is uncertain.

Population-based Methods: These methods simultaneously explore different parts of the design space using a population of candidate solutions, often guided by nature-inspired heuristics (e.g., ant colony, bird swarms, or evolution [39]). Genetic Algorithm (GA), inspired by Darwinian evolution, is the most widely used SS design method due to its ease of implementation. The population evolves through stochastic operations like selection, crossover, and replacement, gradually converging towards a SS that matches target LPs and follows design guidelines.[3] Earlier implementations, such as OptiBLESS (Optimisation of BLEnded Stacking Sequence [13]), enforced guidelines like disorientation solely through penalties. Nevertheless, this does not guarantee that the offspring populations inherit the traits. Newer implementations, such as pyTLO (python Tapered composite Laminate Optimisation [41]), encode these guidelines as constraints, ensuring offspring populations stay guideline-compliant even after genetic operations. However, with increasing number of layers and using finer angle resolutions ([Δ15°]), GAs become computationally expensive, requiring larger populations to preserve diversity and avoid local minima. These demands make GAs less practical.

Layerwise methods: These methods sequentially design SS layer-by-layer. Narita et al. [42,43] used a simple 1D enumeration process,

Table 2

Optimisation problem in focus.

	Description
Objective	minimise ΔLPs (mismatch between desired and realised stiffness)
Variables	**SS**: $[\theta_1, \theta_2, \ldots, \theta_{N/2}]_S$, $\theta \in [\Delta 45°]$ or $[\Delta 15°]$
Constraints	Symmetry, Balanced, 10% Rule, Damage Tolerance, Disorientation, Contiguity (**Design Guidelines**)

selecting the optimal orientation of every layer to minimise mismatch between desired and realised LPs. However, greedy selection for every layer need not guarantee a global optimum solution. This problem was then reformulated as a decision tree with branch-and-bound (BB) optimisation, to explore a broader solution space. The fractal branch and bound (FBB) method [44–46] utilised the fractal nature of LP space, showing how each angle choice influences the realisable LPs. It enabled informed selection of angles, while pruning infeasible branches or guideline-violating partial SS solutions. As the evaluation cost of this method increased heavily with problem size, Liu et al. [47] used a simpler objective function (least square difference of LP mismatch) to improve search speed at the expense of optimality. They mitigated this trade-off by redesigning the SS multiple times. Fedon et al. [48] improved this workflow with LAYLA (LAY-ups for LAminates), which uses beam search, a group-wise redesign strategy, and a computationally efficient method to enforce design guidelines (RELAY [49]). Beam search explores multiple solution branches in parallel to avoid greedy selection. Then, the SS is divided into multiple groups and iteratively redesigned to reduce mismatch. LAYLA can design even 300-layer SSs in few minutes, while adhering to design guidelines. While it scales well for conventional laminates ([Δ45°]), its effectiveness decreases for non-conventional laminates ([Δ15°]), where reported results indicate a four-fold increase in computation time and a significant drop in solution quality.

Amongst state-of-the-art methods, BB offer the best trade-off between efficiency and solution quality. With increasing problem dimensionality, GAs incur high computational costs, while MILP lacks solution quality. BB's strength lies in pruning the search tree to significantly reduce the portion of the design space explored. Pruning can be either *informed* [44] (precise but expensive), or *heuristic* [47,48] (faster but sub-optimal). While heuristic exploration strikes a sufficient balance between solution quality and efficiency with [Δ45°], this advantage visibly diminishes with [Δ15°]. Here, mismatch errors increase due to the limited exploration of a larger design space, and computational times rise with the evaluation of more fibre angle combinations. While BB still outperforms other methods under these conditions, this remains a key limitation. Table 1 collectively presents all these inferences.

As such, state-of-the-art methods still face the challenge of designing an N-layer SS to match input LPs while using a wide range of angles ([Δ15°]) and adhere to all relevant design guidelines. With the advent of comprehensive multi-disciplinary [50] and multi-fidelity [51] optimisation methods, computational limits like this can hinder the depth of design trade studies, resulting in heavier or suboptimal structures. This gap highlights the need for an efficient SS design approach that does not compromise on optimality, as tabulated in Table 2. To address this
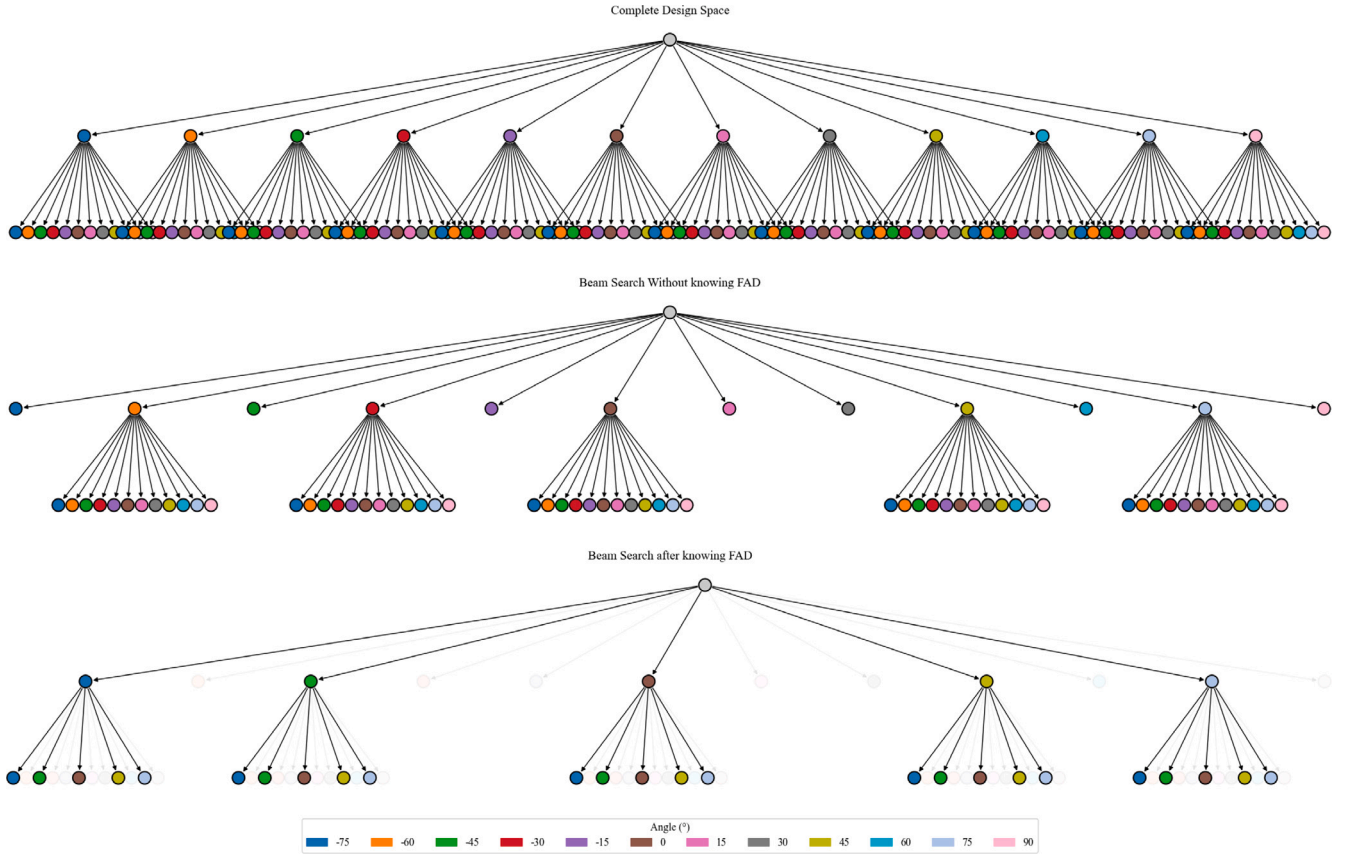
---

[3] See [40,41] for details on encoding SS and design guidelines with GA operators.

Fig. 2. Illustrative comparison of different BB trees for SS design. (Top) All combinations. (Middle) Beam search expands a subset of promising nodes. (Bottom) Beam search with further reduced nodes, excluding angles outside a FAD. Translucent nodes do not contribute to computation.

need, this paper presents a novel, computationally efficient methodology for SS design, even with increased dimensionality. The following section outlines the key concepts behind the proposed method.

3. Proposed methodology for efficient and scalable stacking sequence design from lamination parameters

BB methods reduce computational cost through pruning, but at the expense of limiting the explored design space and compromising solution quality [48]. As a result, this study focused on enriching the design process, rather than limiting it. This enrichment was achieved by introducing an intermediate step: the design of a fibre angle distribution (FAD), which specifies the number of plies oriented at different angles.

Once determined, the FAD serves as an informative guide for SS design, with minimal computational overhead. This effect is illustrated in Fig. 2: the top shows a full BB tree with all nodes expanded, the middle shows beam search reducing the number of explored nodes, and the bottom demonstrates how FAD knowledge further focuses the search by guiding ply angle selection only from a designed set. This reduces computational effort even before pruning, while still making informed choices. Additionally, design guidelines — such as symmetry, balance, and the 10% rule — can be accounted for solely through FADs, further reducing the burden on a BB optimiser.

To enable this FAD-guided approach, this study introduces an efficient method to design them. Since FADs do not encode any through-thickness information and solely describe in-plane stiffness (A), they are sufficiently represented using V^A LPs:

$$V^A = \frac{1}{N}[(N_1 * t(\theta_1)) + (N_2 * t(\theta_2)) + (N_3 * t(\theta_3)) + \cdots .] \quad (3)$$

This formulation resembles a Fourier Series: a function is expressed as a weighted sum of sinusoidal components. Here, the trigonometric function $t(\theta_i)$ captures the stiffness contribution at angle θ_i, and the coefficients N_i represent the number of plies—i.e., the FAD. Based on this analogy, Fast Fourier Transforms (FFTs) were repurposed for laminated composite design. While FFTs are typically used to identify the magnitude of different frequencies in a signal, here, they were used to determine the number of plies at different orientations (their FAD).

This leads to a two-step solution to the inverse problem of converting LPs into SS. First, FFTs enable a fast and elegant derivation of FADs from V^A LPs (LP2FAD). Second, a simple yet robust BB implementation, guided by the FAD, can design a SS to match given V^D LPs (FAD2SS). These two deterministic sub-problems, leveraging well-known mathematical techniques, form the basis of the proposed methodology. This method is encapsulated and published open-source as a Python package named **LP2SS** [52] (lamination parameters (**LP**) to (**2**) stacking sequences (**SS**)), reflecting its overall functionality.

The remainder of this paper is organised as follows: Section 4 explains the implementation of LP2SS (see Fig. 3), which is then evaluated against the state-of-the-art in Section 5. Section 6 discusses the results and demonstrates how LP2SS enables designs with [Δ15°], which are typically difficult and computationally expensive to realise. These findings are then consolidated with conclusions in Section 7 .

4. Implementation of LP2SS

For the inverse problem of converting LPs to SS (LP2SS), the proposed method follows two steps: FAD design and SS design. The following subsections detail the implementation of the novel FFT-based method behind LP2FAD, and then the robust BB method behind FAD2SS.
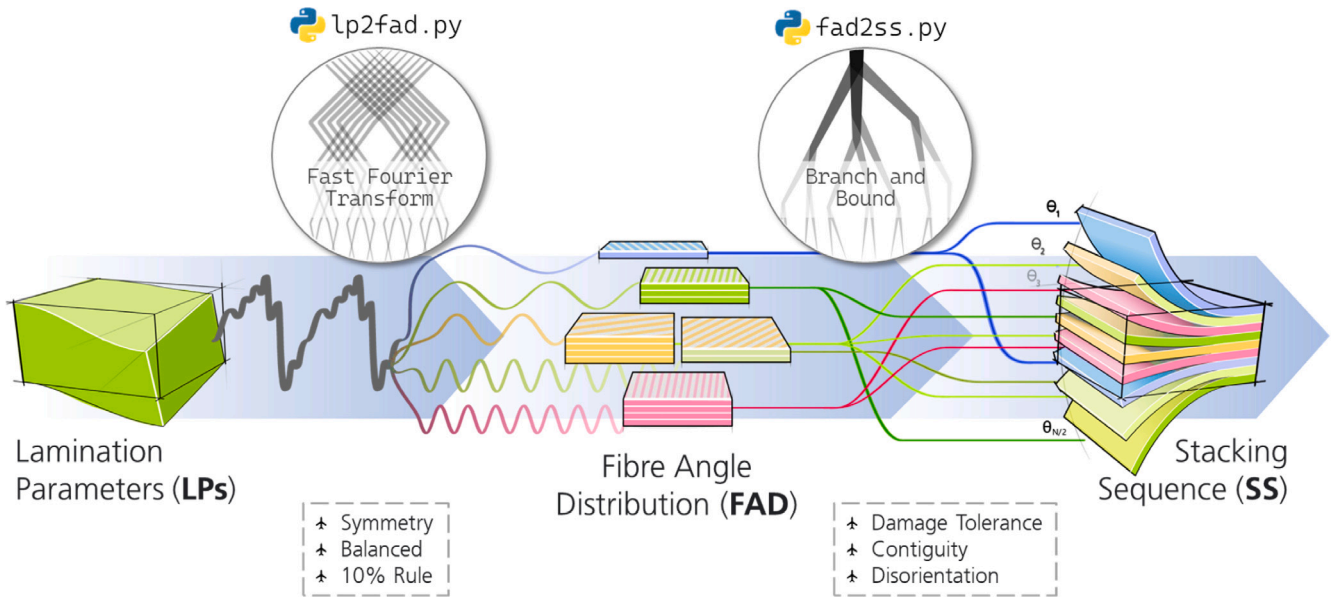
Fig. 3. LP2SS: Proposed methodology to convert LPs into SS (lp2ss.py = lp2fad.py + fad2ss.py).

4.1. Step 1: LP2FAD - From lamination parameters to fibre angle distribution

This subsection outlines how FFTs are performed on V^A LPs to design the FAD of a N-layer SS. The process starts by writing V^A as a signal. Since multiple unique FADs can share the same V^A, multiple valid signal forms can exist. Hence, these periodic signals, composed of sinusoids with repeating patterns, were studied and parameterised with V^A LPs. This approach allowed efficient design of multiple FADs for the same V^A. Having this multiplicity is essential to avoid overfitting and preserve the overall solution quality of LP2SS: a single FAD may perfectly match a given V^A (in Step-1), but can lack the necessary angles to match given V^D LPs (later in Step-2). Since FFT outputs need not be integers, post-processing is done to round ply counts to integers summing to N, while enforcing design rules.

4.1.1. Signal representation of V^A lamination parameters

FFTs can be used to estimate the magnitude of different frequencies in a signal. For FAD estimation, V^A was reinterpreted as a signal (L^A) whose frequency and magnitude corresponded with fibre angles and their ply counts, respectively. Mathematically, the argument of a sinusoid is a product of frequency and time [53]. Hence, a fictitious time variable T was inserted into the V^A LP formulation:

$$V_{1,2}^A = \frac{1}{N} \sum_{k=1}^{N} [\cos(2\theta_k), \cos(4\theta_k)] \Leftrightarrow L^A(T) = \frac{1}{N} \sum_{k=1}^{N} [\cos(2\theta_k T)] \qquad (4)$$

$$\underbrace{\phantom{V_{1,2}^A = \frac{1}{N} \sum_{k=1}^{N} [\cos(2\theta_k), \cos(4\theta_k)]}}_{\text{Normal Representation}} \qquad \underbrace{\phantom{L^A(T) = \frac{1}{N} \sum_{k=1}^{N} [\cos(2\theta_k T)]}}_{\text{Signal Representation}}$$

Due to the focus on Symmetric-Balanced laminates, only the cosines in $V_{1,2}^A$ LPs are focused on. As such, this parameterisation writes $V_{1,2}^A$ as a laminate signal L^A, where the arguments 2θ and 4θ are now harmonically related.

To apply FFT on the laminate signal L^A, its values must be described (sampled) over discrete steps of the fictitious T domain. An appropriate sampling rate and number of samples ($\mathcal{N}$) are critical to ensure reliable FFT results without aliasing. As per the Nyquist-Shannon theorem [54], the sampling rate must be at least twice a signal's highest angular

frequency — equating to 1 sample per second for the given parameterisation.[4] The value $\mathcal{N}$ must be chosen to capture one full period of a signal. As illustrated in Fig. 4, periodicity can vary based on a signal's constituent frequencies (or, angles in this case):
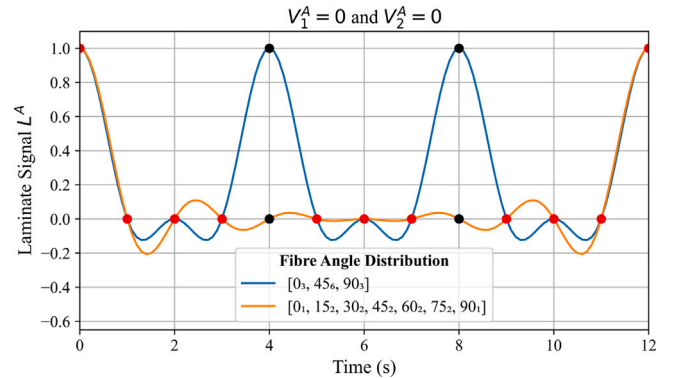

Fig. 4. L^A of two unique 12-layer FADs with same V^A LPs. Sampled points with identical values are marked red, and rest in black.

As seen in Fig. 4, the laminate signals of FADs consisting [$\Delta45°$] and [$\Delta15°$] angles exhibit distinct periodicity. and symmetries. The [$\Delta45°$] FAD exhibits a period of 4, thus requiring $\mathcal{N} = 5$ samples (at $T = [0, 1, 2, 3, 4]$). Meanwhile the [$\Delta15°$] FADs exhibit a period 12, requiring $\mathcal{N} = 13$ samples (at $T = [0, 1, 2, 3, 4, 5, 6, 7, \ldots, 12]$).

By simple substitution in Eq. (4), it can be understood that L^A numerically equals $1, V_1^A, V_2^A$, at $T = [0, 1, 2]$. Moreover, the mid-period symmetry implies that the values at $T = 1$ and $T = 3$ are identical for [$\Delta45°$]. The pattern then repeats beyond $T = 4$. Hence, the signal pattern for [$\Delta45°$] can be tabulated as follows (in Table 3):

Table 3
L^A Signal Pattern for [$\Delta45°$] laminates.

Angle Increments	$T = 0$	$T = 1$	$T = 2$	$T = 3$	$T = 4$	$T > 4$
[$\Delta45°$]	1	V_1^A	V_2^A	V_1^A	1	repeated

---

[4] Sampling Rate and periodicity calculation detailed in Appendix B.1.

Table 4
Exact signal pattern for laminates made of $[0°, 15°, 30°]$ orientations.

Orientations	$T = 0$	$T = 1$	$T = 2$	$T = 3$	$T = 4$	$T = 5$	$T = 6$
$[0°, 15°, 30°]$	1	V_1^A	V_2^A	$6.46 - 10.19V_1^A + 4.73V_2^A$	$20.39 - 30.58V_1^A + 11.19V_2^A$	$35.32 - 51.98V_1^A + 17.66V_2^A$	$41.78 - 61.17V_1^A + 20.39V_2^A$

For $[\Delta 15°]$, similar use of substitution and symmetries is not sufficient to describe the entire sample set, as values at $T = [3, 4, 5, 6]$ still need to be determined. This problem was handled in two different ways. Their values can be analytically determined, or manually approximated as a function of V^A LPs. These two types formed the basis of a database of pre-observed patterns. This database evolved throughout the study until a desired number of diverse solutions could be generated. The sufficient number of patterns was determined later in Section 4.2.3, through actual SS design attempts with $[\Delta 15°]$.

Analytical Exact Patterns: To analytically determine values of L^A at any given T, they were described as a linear combination of the known quantities $L^A(T = [0, 1, 2])$:

$$L^A(T) = a_T \left(L^A(T = 0) \right) + b_T \left(L^A(T = 1) \right) + c_T \left(L^A(T = 2) \right)$$
$$\Rightarrow L^A(T) = a_T + b_T V_1^A + c_T V_2^A \tag{5}$$

Upon assuming a set of three ply orientations to be used (similar to the three-layer logic of Hammer [25]), the coefficients a_T, b_T, and c_T can then be solved for a given value of T, by equating Eqs. (4) and (5)[5]:

$$\begin{bmatrix} a_T \\ b_T \\ c_T \end{bmatrix} = \begin{bmatrix} 1 & \cos(2\theta_1) & \cos(4\theta_1) \\ 1 & \cos(2\theta_2) & \cos(4\theta_2) \\ 1 & \cos(2\theta_3) & \cos(4\theta_3) \end{bmatrix}^{-1} \begin{bmatrix} \cos(2\theta_1 T) \\ \cos(2\theta_2 T) \\ \cos(2\theta_3 T) \end{bmatrix} \tag{6}$$

Thus, using Eq. (6), the value of the signal can be exactly calculated for any timestamp T. From $[\Delta 15°]$, a set of three angles can be chosen in $^7C_3$ ways ($\because$, seven unique $|\theta|$ exist within $[\Delta 15°]$). Ergo, 35 'Exact' signal patterns can be formulated. For example, the exact pattern for $[0°, 15°, 30°]$ is shown in Table 4. The pattern is described only up to $T = 6$ due to the signals' mid-period symmetry. For brevity, the complete list of Exact patterns is presented in the Appendix (Table 11).

Manual Approximate Patterns: To design FADs with more than three unique angles, exact patterns are infeasible. Hence, signal patterns were approximated with V^A LPs using visual pattern matching. This approach inherently fixes the contributions of some ply orientations, while others (typically three) remain designable. While this can be done in innumerable ways, the signal representation helps handle this situation with ease. This visual pattern approximation exercise can be explained with the following example. A combination $V_{1,2}^A = [0.17, -0.1]$ was randomly chosen from the feasible V^A LP space. From an in-house laminate database[6], multiple FADs made of $[\Delta 15°]$ that match these LPs were noted. Their corresponding L^A signals were then plotted for analysis in Fig. 5.

In Fig. 5, the signal values at timestamps $T = 4$ and 5 are equal, while a variation can be observed at timestamps $T = 3$ and 6. Nevertheless, these common and uncommon points (at $T > 2$) were manually approximated as a function of V^A LPs. However, the sample value at $T = 3$ and 6 can be represented by multiple equivalent V^A parameterisations. In such cases, the most effective approximation was chosen by perturbing the reference FAD's ply counts and identifying which yielded the closest matching signal. In this manner, a manually approximated FAD can be made as shown in Table 5.

By repeating this exercise with laminates from across the design space, several 'Approximate' patterns for $[\Delta 15°]$ were made.
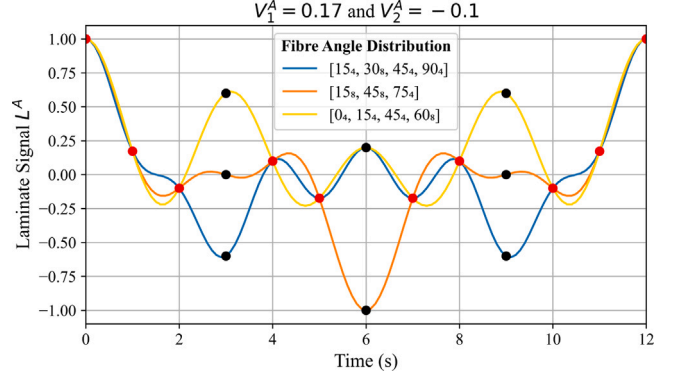

Fig. 5. L^A Signals of FADs corresponding to $V_{1,2}^A = [0.17, -0.1]$. Sampled points with equal values across all the FADs are marked in red.

Table 5
Approximate Signal Pattern corresponding to $V_{1,2}^A = [0.17, -0.1]$.

$T = 0$	$T = 1$	$T = 2$	$T = 3$	$T = 4$	$T = 5$	$T = 6$
1	V_1^A	V_2^A	0	$-V_2^A$	$-V_1^A$	$-2V_2^A$

4.1.2. Deriving fibre angle distribution from the fast fourier transform of laminate signals

For a target set of V^A LPs, different periodic signals can be created using pre-observed patterns. Applying FFT on them paved the way for efficiently designing multiple unique FADs. For an example case ($V_{1,2}^A = [0.52, 0.15]$ and $N = 20$), the pattern in Table 5 yield the following frequency spectrum in Fig. 6.

Fig. 6. Frequency Spectrum of L^A ($V_{1,2}^A = [0.52, 0.15]$ and $N = 20$): FFT magnitudes (left y-axis), and Number of Plies (right y-axis).

Only the positive real components of the spectrum are considered, as imaginary or negative FFT values (if present) have no physical meaning in the laminate signal parameterisation used here. The spectrum is then normalised by dividing each value by the average FFT sum per layer (total sum of FFT values divided by N). The resulting FAD (for all $|\theta|$) is listed in Table 6.

Since $V_{1,2}^A$ are composed of cosine terms, the fibre orientation θ is invariant to sign; that is, $+\theta$ and $-\theta$ contribute equally. Consequently,

---

[5] An expanded derivation of this solution is presented in Appendix B.2.
[6] This was generated via brute-force enumeration for $N = 5$ till 15 and is published alongside this study [55].

Table 6

FAD ($\forall\ |\theta|$) obtained from L_1^A ($V_{1,2}^A = [0.52, 0.15]$ and $N = 20$).

Ply Orientation (°)	0	15	30	45	60	75	90
Ply Count	4.91067	5.488	4.57733	3.33333	0.08933	1.17866	0.422667

Table 7

Analysing a non-integer FAD ($\forall |\theta|$) obtained from FFT of L^A made of: $V_{1,2}^A = [0.52, 0.15]$ and $N = 20$.

Ply Orientation (°)	0	15	30	45	60	75	90	Sum
Ply Count	4.91067	5.488	4.57733	3.33333	0.08933	1.17866	0.422667	20
Even Integer	4	4	4	2	0	0	0	14
Residual	0.91067	1.488	0.57733	1.33333	0.08933	1.17866	0.422667	6

Table 8

Symmetric-Balanced FAD ($\forall |\theta|$) obtained from L^A ($V_{1,2}^A = [0.52, 0.15]$ and $N = 20$) using an Approximate Pattern.

Ply Orientations (°)	0	15	30	45	60	75	90
Ply Count	4	6	6	2	0	2	0
Mismatch Error ϵ_A	0						

ply counts are expressed as $|\theta|$, combining contributions from both $+\theta$ and $-\theta$. In this example, the ply counts sum to the desired $N = 20$, yielding LPs $V_{1,2}^A = [0.52, 0.15]$. As such, a FAD for any value of N can be inferred from the FFT results upon normalisation. However, non-integer ply counts must be corrected for manufacturability. Additionally, design guidelines such as balance and the 10% rule must be met. Therefore, additional post-processing of the FAD is necessary.

4.1.3. Enforcing manufacturability and design guidelines for fibre angle distribution

When the FAD obtained from FFT contains non-integer ply counts, a rounding procedure is applied to ensure manufacturability. This process ensures that off-axis $|\theta|$ values are balanced while maintaining a total of N plies. This is illustrated using the FAD example from Table 6, where each ply count is first decomposed into its even-integer and residual (fractional) components, as shown in Table 7. An emphasis is placed on having even ply counts, so that $|\theta|$ can be equally split between $+\theta$ and $-\theta$, for a balanced solution.

Here, the even components sum to 14, meaning six additional plies must be added to reach the required $N = 20$. This was done by rounding up ply counts while ensuring the off-axis plies remain balanced. In this case, 112 valid rounding combinations are possible.[7] Optionally, this step can also consider sign-sensitive angle bins (i.e., treating $+\theta$ and $-\theta$ as distinct rather than the aggregated $|\theta|$). This allows for a broader set of combinatoric possibilities — potentially resulting in FADs that are mathematically in-plane orthotropic — even without enforcing the balanced laminate rule.

Each rounded FAD was then evaluated based on its closeness to the target laminate parameters, using Euclidean distance:

$$\epsilon_A = \sqrt{\sum (|V_{Design}^A - V_{Target}^A|)^2} \tag{7}$$

V_{Design}^A is computed from each rounded FAD and V_{Target}^A is the original design target. The FAD with the lowest error was selected, as shown in Table 8.

Symmetry was enforced by determining the FAD for one-half of the laminate. For odd-symmetric cases, the same procedure is followed while allowing one angle to have an odd-ply count, which is the middle ply. For the balanced rule, off-axis ply counts ($|\theta|$) are evenly split between $+\theta$ and $-\theta$. If the 10% rule is desired, the same number of plies

is preallocated to [0°, ±45°, 90°], and the remainder of the FAD is designed to match the given V^A. For non-conventional angle sets ([$\Delta 15°$]), only the LP-based formulation of the 10% rule is considered [22].

4.2. Step 2: FAD2SS - from fibre angle distribution to stacking sequences

Once multiple FADs are designed in Step 1 (LP2FAD), the top four solutions are selected to be converted to SS in Step 2 (FAD2SS). A BB algorithm with beam search was developed to optimally assign the through-thickness positions of the plies in the FAD. After this, an open-source laminate repair tool was employed to enforce design guidelines for the SS.

4.2.1. Designing stacking sequence with branch and bound

In this study, a BB algorithm was implemented in Python to design SS from a given FAD. As motivated earlier (Section 3), BB treats SS design as a decision tree search problem, by designing SS layer by layer. The beam search method allowed simultaneous evaluation of multiple solution branches, guided by a heuristic cost function defined as the mean squared error between the obtained and desired V^D LPs.

$$\epsilon_D = \frac{1}{4} \sum (|V_{Design}^D - V_{Target}^D|)^2 \tag{8}$$

This formulation was chosen over the previously used Euclidean distance (Eq. (7) in Step-1) to reduce computational burden: LP mismatch can be computed incrementally for a (partially) designed SS by adding each layer's contribution, without repeatedly computing a fourth root.

To ensure ease of use and repeatability, the implementation was kept free of tuning or hyperparameters (e.g., branching limits or refinement cycles). The number of simultaneously explored solutions in beam search (beam width) was suitably fixed[8] to avoid sensitivity to hyperparameter tuning.

4.2.2. Enforcing design guidelines for stacking sequence

The design guidelines to enforce at this stage are Damage Tolerance, Disorientation, and Contiguity. Damage Tolerance can be addressed by constraining the outermost ply angle to 45°, while the others require more nuanced handling. Initial efforts to enforce them using pruning in the BB method (in Section 4.2) limited design space exploration and often led to local optima. A posterior repair strategy was therefore adopted, using RELAY [49], an open-source Python-based tool.

RELAY minimally modifies a SS designed by FAD2SS — mainly through ply shifts and, if necessary, angle changes — to enforce guidelines like Disorientation and Contiguity, while preserving the target V^A and V^D LPs [49]. Its effectiveness depends on three hyperparameters: nD1 (number of redesigned plies), nD2 (ply shifts tested to reduce V^D mismatch), and nD3 (repetitions of the shift algorithm). The developer recommended default values (nD1 = 6, nD2 = 10, nD3 = 2) to balance computational cost and repair success. However, since repairs are not

---

[7] This combinatoric was based on distributing six additional plies (as three balanced pairs), across seven absolute angle bins.

[8] Testing across a range of values showed performance converging at a beam width of 10.

always successful, this study uses an adaptive strategy: if the repair fails, nD1 was increased by two and retried (up to five times).

4.2.3. Assuring stacking sequence solution diversity

As discussed earlier, a FAD matching the desired V^A LPs need not contain fibre angles that help match the desired V^D LPs. Therefore, in LP2FAD, multiple FADs are created using a database of pre-observed signal patterns. However, the sufficiency of this database must be validated through actual SS design attempts to ensure the desired solution diversity across various ply counts and the enforcement of desired design guidelines. Hence, an exhaustive validation process was undertaken.
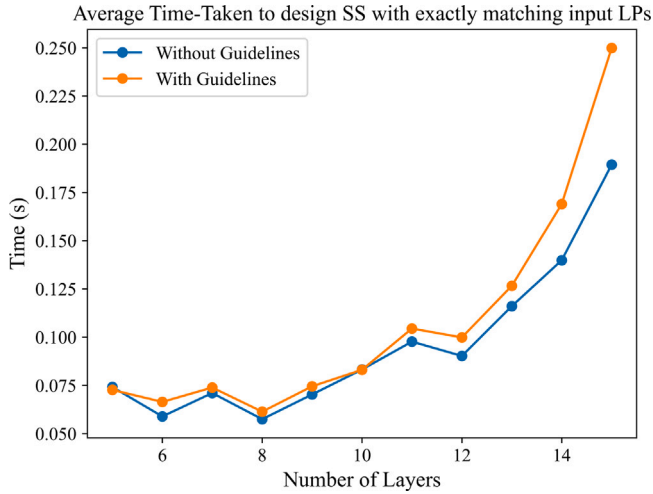

Fig. 7. LP2SS with a database of 66 signal patterns, sufficient to exactly match all possible SS for $N = 5, 6, 7, 8, \ldots, 15$ (1.6 million SS).

To this end, all symmetric and balanced SS from $N = 5$ to 15 with $[\Delta 15°]$ were enumerated—approximately 1.6 million unique sequences. For each SS, corresponding LPs and compliance with the design guidelines (10% Rule, Disorientation, Damage Tolerance, and Contiguity) were noted to form a reference test dataset. Mismatch error from here onward will be represented as a mean squared error between the designed and target LPs (V_1^A, V_2^A, V_1^D, V_2^D, V_3^D, and V_4^D). This metric was chosen to be consistent with previous comparative studies [48].

$$\varepsilon = \frac{1}{6}\sum(|V_{Design}^{A,D} - V_{Target}^{A,D}|)^2 \qquad (9)$$

For a given case, if LP2SS failed to design a SS with mismatch error[9] below 10^{-2} and satisfy applicable guidelines, new signal patterns were added by manually analysing the corresponding enumerated SS and parameterise their signal pattern with LPs. This approach helped identify a robust pattern database to design any N-layer SS, with the angular diversity to help satisfy design guidelines.

Ultimately, a total of 66 unique signal patterns (listed in Appendix B.3) sufficed to design all test cases with exact LP matching (mean squared error $\approx 10^{-35}$) and guideline-compliance. Fig. 7 shows each case was solved within a few tenths of a second on average. With multiple FADs available, the implementation readily supports designing multiple unique SS, efficiently enabling alternative designs on demand. Since the methods within LP2SS are deterministic and scalable, this validation over small N values ensures robust and diverse solutions with increasing dimensionality. The following subsection demonstrates LP2SS on a representative mechanical design problem.

---

[9] A mismatch limit of mean squared error 10^{-2} was conservatively estimated from design case studies seen in literature [56,57].

4.3. Demonstration on a loaded plate design case

This subsection illustrates the use of LP2SS in the optimisation of a loaded composite plate. The case, adapted from Liu et al. [47], considers a simply supported rectangular plate of dimensions 100 mm $\times$ 150 mm, designed for a buckling load of 100 kN (longitudinal compression). The plate stiffness was optimised using LPs, with the software *VICONOPT* [58], resulting in the following target vectors:

$$V^A = [-0.1196, -0.0585, 0, 0],$$

$$V^D = [0.0483, -0.721, -0.0196, 0.0], \quad N = 28$$

For complete details of the plate setup and LP optimisation, readers are referred to the original study [47]. Using these LP targets, the proposed LP2SS method was used to design the loaded plate. Table 9 summarises the resulting SS for varying sets of imposed guidelines, along with the corresponding runtimes and LP-mismatch (as defined in Eq. (9)).

Table 9
LP2SS results for the simply supported loaded plate design case.

Design Guidelines	Resulting SS	Time (s)	Error ε
Symm + Bal + 10% Rule	$[45, 45, 0, -45, -45, -45, -45,$ $0, 45, 45, 90, 90, 90, 90]_S$	0.29	1.04E−05
Symm + Bal + 10% Rule + Contiguity	$[-45, 45, 45, -45, -30, 30, 60,$ $-60, 0, -75, 0, 90, 90, 75]_S$	0.41	1.20E−05
Symm + Bal + 10% Rule + Disorientation + Contiguity	$[-45, -45, 0, 45, 45, 30, 60,$ $75, -60, 90, 90, -75, -30, 0]_S$	0.57	1.76E−03

Across all cases, LP2SS consistently designed laminates that satisfy the imposed guidelines within sub-second runtime while maintaining the target stiffness with negligible mismatch. This example demonstrates the method's practical applicability in efficiently translating optimised LPs into SS. The following section further evaluates its robustness and comparative performance against state-of-the-art methods.

5. Comparison of LP2SS with state-of-the-art

This section compares LP2SS with established SS design methods across varying problem sizes and complexities. The evaluation uses benchmark datasets with LPs spanning diverse regions of the design space, effectively representing optimal solutions for various mechanical problems. The objective is to assess each method's ability to design guideline-compliant SS for all cases with minimal runtime and low LP mismatch.

Methods Evaluated: These include GA, BB, MILP, and LP2SS (the proposed method). OptiBLESS [13] and pyTLO [41] (GA), LAYLA [48] (BB), DMRG [37] (MILP using quantum-inspired solver). OptiBLESS and pyTLO are used for $[\Delta 45°]$ and $[\Delta 15°]$ designs, respectively, due to their respective limitations in initial population generation with design guidelines. DMRG was tested exclusively with $[\Delta 45°]$, as the current implementation supports only this configuration while adhering to design guidelines. Given the nondeterministic nature of MILP and GA implementations, they were run multiple times, and the best solution was presented. The hyperparameters used for all State-of-the-art methods are listed in Appendix B.5.

Benchmark Datasets: Tests were conducted using two benchmarks, each containing 100s of guideline-compliant SS across varying ply counts. Since the LPs corresponding to these SS are realisable, all design methods can be expected to recreate these SS, or equivalent ones, that satisfy all constraints. The benchmark from the University of Bristol [14], contains 200 SS with $[\Delta 45°]$ angles for each $N = [40, 80, 200]$. However, it lacks LP values attainable only with finer angle resolutions. This gap is addressed by introducing a new benchmark in this study [55], comprising over 450 SS for each ply count with $[\Delta 15°]$ angles, for $N = [10, 20, 40, 80, 100, 200]$. Compared to the

Table 10

Test Matrix for Evaluating LP2SS and State-of-the-Art Methods.

Criteria	Bristol Benchmark [14]	Newly Proposed Benchmark [55]
Composition	LPs from SS with [$\Delta45°$] angles	LPs from SS with [$\Delta15°$] angles
Ply Counts (N)	40, 80, 200	10, 20, 40, 80, 100, 200
Admissible Angles	[$\Delta45°$], [$\Delta15°$]	[$\Delta15°$] only
Methods Evaluated	GA (OptiBLESS, pyTLO), BB (LAYLA), MILP (DMRG), LP2SS	GA (pyTLO), BB (LAYLA), LP2SS
Design Guidelines	Symmetry, Balance, 10% Rule, Disorientation ($\Delta\theta \leq 45°$), Contiguity (max 5 plies)	

Bristol benchmark, these datasets represent a more diverse spread of stiffness combinations across the design space — as evident from the LP projection plots provided in Appendix B.4.

Evaluation metrics: Performance across a range of N was assessed using two metrics: (i) LP mismatch error and (ii) Computational time. As different methods operate well with different objective functions (e.g., root mean square error, or absolute error), the mean squared error (Eq. (9)) of all solutions were used for consistent comparisons. The tests enforce all key design guidelines: Symmetry, Balance, Disorientation ($\Delta\theta \leq 45°$), Contiguity (max. five plies), and the 10% rule. For non-conventional angles, the ply-count-based 10% rule is replaced with the LP-based formulation from Abdalla et al. [22], which ensures the designed V^A LPs lie within a feasible domain. The complete test plan is summarised in Table 10.

5.1. Performance evaluation with existing benchmarks

Each case from the Bristol datasets (200 cases for each $N = 40$, 80, and 200) was provided as an LP target to the design methods. Although originally derived from a [$\Delta45°$] SS, these targets were also attempted to be designed using [$\Delta15°$][10], to evaluate scalability. Figs. 8(a) and 8(b) present the trends in LP mismatch error and runtime for both angle sets.

These evaluations reaffirmed the trends noted in the literature review. GAs like OptiBLESS and pyTLO struggle to consistently make guideline-compliant SS without incurring high LP mismatch errors and long runtimes. Although pyTLO shows decreasing mismatch errors with increasing N ($\because$, greater design freedom), it remains inefficient. DMRG (MILP), though nondeterministic, offers slightly faster runtimes than LAYLA (BB) but incurs higher mismatch errors. LAYLA (BB) and LP2SS show comparable solution quality when using [$\Delta45°$], but only LP2SS maintains or improves performance when extended to the more vast [$\Delta15°$] space. Unlike the previous section, while testing with fewer layers, LP2SS does not always achieve perfect LP matches, due to the heuristic pruning of its BB method in FAD2SS. Nonetheless, it outperforms other methods, generating precise, guideline-compliant SS in under a second—compared to minutes required by state-of-the-art alternatives. This superior scalability is more evident when considering the total time taken to complete the Bristol benchmark. While other tools require at least 20 hrs, LP2SS completes this test suite in under 20 mins.

5.2. Performance evaluation with newly proposed benchmarks

To further assess scalability, the newly introduced [$\Delta15°$] benchmarks were used. For these test cases, Fig. 8(c) shows how mismatch error and runtime evolve with increasing N.

LP2SS achieves perfect LP matching for $N = 10$, with runtimes comparable to LAYLA and significantly outperforming pyTLO. The latter highlights a practical lower bound on runtime for GA-based methods, which cannot operate any faster due to their inherent population generation and evaluation overhead. As N grows, both pyTLO

and LAYLA suffer from increased mismatch errors and runtime, often converging to suboptimal solutions — highlighting their limited ability to utilise an expanded design space fully. LP2SS, in contrast, maintains unparalleled computational efficiency and precision across all N, demonstrating its robustness with expanded design spaces.

6. Discussion

6.1. Conventional [$\Delta45°$] vs non-conventional [$\Delta15°$] fibre angles

The use of non-conventional fibre angles $\theta \in [\Delta15°]$ enables better utilisation of a fibre's directional properties, compared to the conventional [$\Delta45°$]. In order to visualise this in terms of the stiffness design space, the V^A LPs were uniformly sampled for symmetric-balanced conditions ($V^A_{3,4} = 0$). LP2SS was then used to attempt designing a solution for each sampled point. Plotting the resulting mismatch errors over these samples reveals the realisable regions of the design space- as shown by the zero error points (in Fig. 9).

Using [$\Delta15°$] enables a broader range of stiffness combinations to be realised with fewer layers, compared to [$\Delta45°$]. These realisable V^A combinations correspond to a FAD, which can be rearranged into different SS with distinct V^D values. LP2SS, with its proven robustness, demonstrates how the [$\Delta15°$] design space is larger and more closely approximates the continuous LP design space than that of [$\Delta45°$].

6.2. Implications of using fast fourier transforms

FFTs provide an elegant and highly efficient way for designing multiple unique laminates with similar stiffnesses. By using a database of pre-observed signal patterns, laminate signals were instantaneously transformed into multiple unique FADs. This supports robust design of guideline-compliant SS.

A key implication of using FFTs is their dependence on a manually curated signal-pattern database. As demonstrated by over 1.6 million test cases (Sections 4.2.3 and 5), the 66 patterns in LP2SS suffice to match stiffness targets and enforce guidelines within tenths of a second, regardless of the layer count. Nevertheless, to achieve the same performance and robustness for a different set of ply orientations (such as [$\Delta5°$]), will require expanding the database through additional manual effort.

6.3. Implications of using a multi-step method (LP2SS = LP2FAD + FAD2SS)

The multi-step architecture of LP2SS — comprising FAD design, SS design, and posterior guideline enforcement — distinguishes it from existing methods. A known caveat of such approaches is the potential for suboptimal interaction between steps: a FAD perfectly matching V^A LPs, may lack the necessary angles for a guideline-compliant SS, matching V^D LPs. For example, a FAD composed of [$0°, \pm60°, 90°$] will inherently violate the disorientation rule. LP2SS manages this situation by designing multiple unique FADs upfront using the signal pattern database. This provides alternative set of ply angle selections, enabling viable solutions. Designing FADs prior to SS design also simplifies the BB implementation. Unlike state-of-the-art BB methods [14,47], LP2SS

---

[10] As [$\Delta45°$] $\subset$ [$\Delta15°$], both sets are valid for the Bristol Benchmark tests.
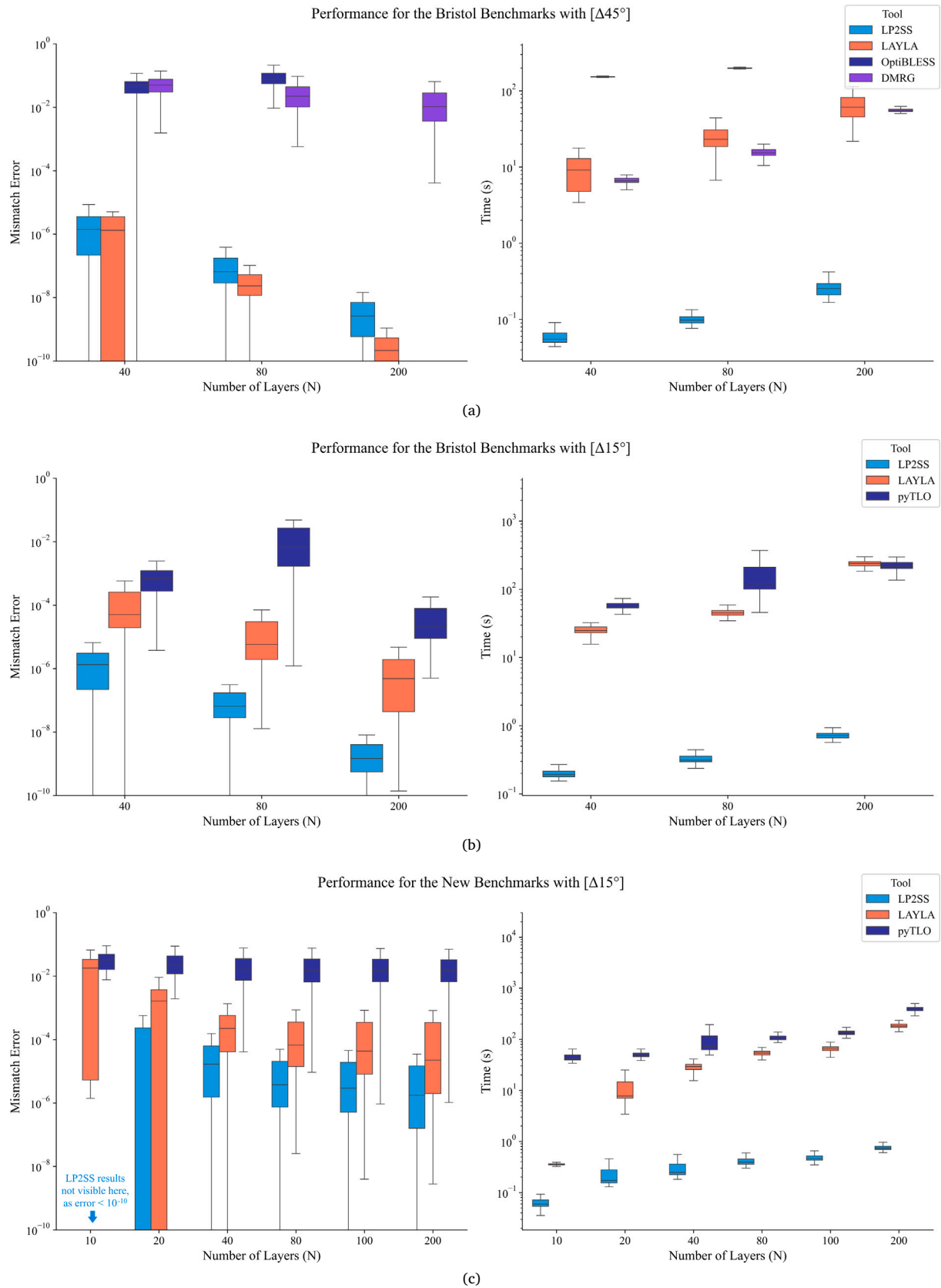
Fig. 8. Comparison of mismatch error and time taken by various methods across all benchmark datasets.
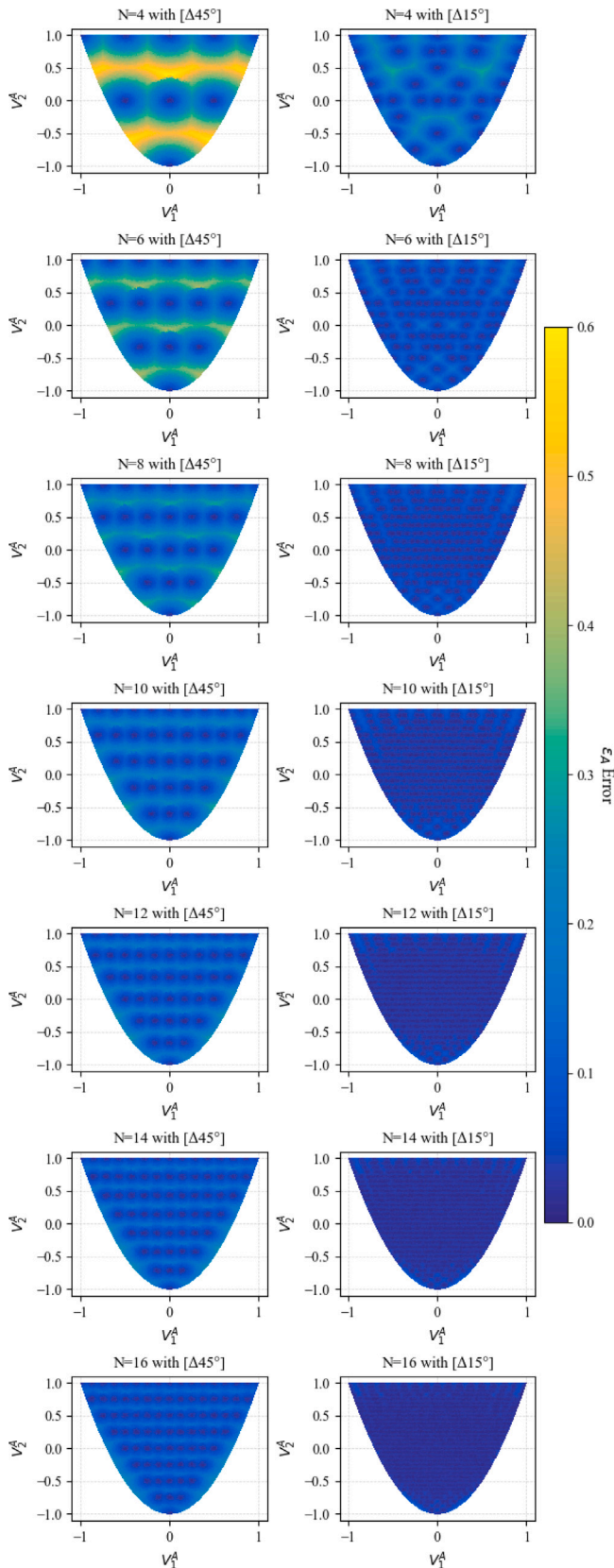
Fig. 9. Design space of Symmetric-Balanced FADs with $N = [4, 6, \ldots, 14, 16]$, compared between $[\Delta 45°]$(left) and $[\Delta 15°]$(right).
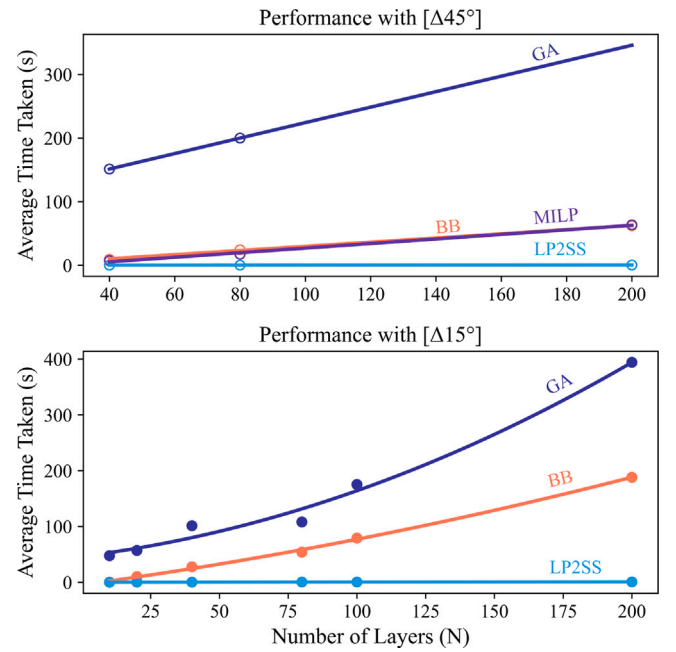

Fig. 10. Computational Performance of all tested methods to design SS from LPs and enforce design guidelines: $[\Delta 45°]$ (top), and $[\Delta 15°]$ (bottom).

avoids dynamic branching limits and groupwise refinements without compromising solution quality.

6.4. Time complexity and scalability of LP2SS

Fig. 10 presents the computational performance of all tested methods for guideline-compliant SS design from LPs. Unlike other methods that exhibit linear or quadratic[11] growth in runtime with increasing ply counts, LP2SS consistently achieves sub-second performance across all angle sets. This superior scalability stems from three factors: the innovative use of FFTs for FAD design, a simple yet effective BB implementation, and a combination of pre-observed laminate signal pattern database with efficient programming practices to reduce dynamic memory allocation.

Compared to the many minutes required by state-of-the-art methods, LP2SS achieves sub-second runtimes. Since such methods are typically applied across multiple structural regions or repeatedly within optimisation loops, this efficiency translates into substantial cumulative computational savings, enabling faster trade studies without compromising solution quality.

While conventional sub-laminate or homogenised strategies in industrial workflows (briefly discussed in Appendix A.1) allow for ease of design iterations, they limit simultaneous optimisation of in-plane (A) and out-of-plane (D) stiffness. LP-based designs enable this, offering more efficient load-path tailoring. LP2SS makes such designs practically accessible, marking a substantial advancement in the domain of efficient composite laminate design from conceptual stiffness requirements.

7. Conclusion

This paper presents LP2SS, a novel and efficient approach to address the 'Inverse Problem' of converting Lamination Parameters (LPs) to

---

[11] For brevity, the polynomial regression lines from Fig. 10 are included in Appendix B.6.

Stacking Sequence (SS). The proposed SS design method is deterministic, delivering high accuracy in LP matching while being exceptionally time-efficient. The method is structured as follows: first, the Fibre Angle Distribution (FAD) is created using a novel fast Fourier transform (FFT)-based approach, which then serves as a basis for designing SS using a Branch and Bound method with Beam search. Both steps were accompanied by post-processing to ensure integer ply counts and adherence to design guidelines.

The use of FFTs enabled an elegant way to design multiple unique FADs and eventually SS. While considerable hours were spent manually parameterising signal patterns with LPs, exhaustive testing schemes ensured that LP2SS was robust and ready for practical use in designing SS with [$\Delta15°$]. The use of such fibre angles allows broader portions of the feasible LP design space to be matched with fewer layers, facilitating lighter designs compared to the conventional [$\Delta45°$].

Furthermore, testing against popularly-used genetic algorithms (GA) [13,41], Mixed-Integer Linear Programming (MILP)(with quantum-inspired solver) [37], and branch & bound(BB) [14] methods showed that LP2SS outperforms the state-of-the-art in all metrics. Even with increasing problem dimensionality (increasing N, [$\Delta15°$], and design guideline enforcement), LP2SS consistently provides closely matching results within a second, establishing its efficiency and effectiveness for large-scale composite structural design.

To further develop LP2SS and this line of work, we recommend the following:

- **Application for variable stiffness laminates:** To maximise LP2SS's capability of making multiple unique SS solutions, further development is needed to effectively utilise them while designing variable stiffness with laminate blending [41] or fibre steering [9].
- **Increasing solution diversity:** LP2SS can currently design using the conventional [$\Delta45°$] and non-conventional [$\Delta15°$] angles. Accommodating greater diversity for variable stiffness designs or finer increments (e.g., [$\Delta5°$]) requires manually adding more signal patterns. Automating this signal curation process will ensure robust scalability of LP2SS.

Data availability

The raw data required to reproduce these findings are available to download from [55]. The code is available on a public, open access repository [52].

CRediT authorship contribution statement

Rakshith Manikandan: Writing – review & editing, Writing – original draft, Validation, Software, Methodology, Conceptualization. **D.M.J. Peeters:** Writing – review & editing, Supervision, Conceptualization. **J.M.J.F. van Campen:** Supervision, Conceptualization, Writing – review & editing. **Sascha Dähne:** Validation, Software. **David Zerbst:** Writing – review & editing, Resources, Funding acquisition. **Christian Hühne:** Supervision, Resources.

Declaration of competing interest

The authors declare that they have no known competing financial interests or personal relationships that could have appeared to influence the work reported in this paper.

Acknowledgements

Appendix A. Theoretical background

A.1. Design practices followed in industry

Early design practices relied on sizing pre-defined sub-laminates: homogenised angle sequences that satisfied empirical design rules. These sub-laminates served as building blocks to construct guideline-compliant laminates. The recent concept of Double-Double laminates formalises this strategy using the [$\pm\phi$, $\pm\psi$] building block, enabling rapid, albeit sub-optimal designs [59]. They have also been adopted in gradient-based structural optimisation efforts [60].

Nevertheless, Airbus's optimisation strategy for the A350 demonstrates relatively more design freedom compared to classic homogenisation approaches [61,62]. With a library of optimisation methods in play, their approach first optimises the SS thickness and their ply angle %'s across the structure, assuming a uniform through-thickness distribution of angles. A blended SS is then optimised to meet design guidelines and a minimum reserve factor for different structural failure modes. However, this approach fixes the load paths early (A stiffness), and consequently restrain out-of-plane stiffness tailoring (D stiffness).

A.2. Material invariants

$$\Gamma_0 = \begin{bmatrix} U_1 & U_4 & 0 \\ U_4 & U_1 & 0 \\ 0 & 0 & U_5 \end{bmatrix} \quad \Gamma_1 = \begin{bmatrix} U_2 & 0 & 0 \\ 0 & -U_2 & 0 \\ 0 & 0 & 0 \end{bmatrix} \quad \Gamma_2 = \frac{1}{2}\begin{bmatrix} 0 & 0 & U_2 \\ 0 & 0 & U_2 \\ U_2 & U_2 & 0 \end{bmatrix}$$

$$\Gamma_3 = \begin{bmatrix} U_3 & -U_3 & 0 \\ -U_3 & U_3 & 0 \\ 0 & 0 & -U_3 \end{bmatrix} \quad \Gamma_4 = \begin{bmatrix} 0 & 0 & U_3 \\ 0 & 0 & -U_3 \\ U_3 & -U_3 & 0 \end{bmatrix}$$

Where,

$$U_1 = \frac{1}{8}\left(3Q_{11} + 3Q_{22} + 2Q_{12} + 4Q_{66}\right)$$

$$U_2 = \frac{1}{2}\left(Q_{11} - Q_{22}\right)$$

$$U_3 = \frac{1}{8}\left(Q_{11} + Q_{22} - 2Q_{12} - 4Q_{66}\right)$$

$$U_4 = \frac{1}{8}\left(Q_{11} + Q_{22} + 6Q_{12} - 4Q_{66}\right)$$

$$U_5 = \frac{1}{8}\left(Q_{11} + Q_{22} - 2Q_{12} + 4Q_{66}\right)$$

These Q entities are the reduced material stiffness values:

$$Q = \begin{bmatrix} \frac{E_1}{1-\nu_{12}\nu_{21}} & \frac{\nu_{12}E_2}{1-\nu_{12}\nu_{21}} & 0 \\ \frac{\nu_{12}E_2}{1-\nu_{12}\nu_{21}} & \frac{E_1}{1-\nu_{12}\nu_{21}} & 0 \\ 0 & 0 & G_{12} \end{bmatrix}$$

The reduced stiffness matrix Q can be characterised using five material properties that can be obtained from uniaxial mechanical tests: E_1 (Young modulus in longitudinal (fibre) direction), E_2 (Young modulus in transverse (matrix) direction, G_{12} (In-Plane Shear modulus), v_{12}, and v_{21} (Poisson's ratio). The (1–2) notation used here represent the principal directions of orthotropy.

A.3. Requisites for lamination parameter optimisation

The lamination parameters (LPs) are mathematically described in a continuous and convex design space [17]. Such properties allow the use of time-efficient gradient-based optimisation algorithms. However, that does not easily assure optimality, as the optimisation objectives (structural responses such as buckling, strain failure criterion, aeroelastic requirements, etc. [12]) need not be convex. As a consequence, several studies can be found in the literature that use different gradient-based methods to optimise LPs [9,63,64]. Moreover, appropriate optimisation constraints need to be used to account for the following: mathematically feasible domains of LPs, correlations between them, and the practically realisable regions of LPs upon following design guidelines. This is still an actively studied topic in literature, and an appropriate list of constraints can be referred from [22,23,63,65].

For completeness, it is noted that, analogous to how LPs help optimise stiffnesses under Classical Laminate Theory, an alternative formulation — Polar Parameters — can be used for First-order Shear Deformation Theory based stiffnesses [66].

Appendix B. Implementation

B.1. Sampling requirements for FFT of laminate signals

To avoid aliasing and ensure reliable FFT outputs, a signal must be appropriately sampled. The Nyquist-Shannon theorem was followed to achieve the same [54]. For the parameterisation used to represent V^A LPs as signals (in Eq. (4)), frequency corresponds with 2θ, and $\theta \in (-90, 90]$. Hence, the highest frequency is $2 * 90°$ or $\pi\ rad$. As such, the sampling rate in fictitious time T can be quantified as follows:

Sampling Rate $\geq 2 *$ Highest Angular Frequency in Signal

$\Rightarrow$ Sampling Rate $\geq 2 * \dfrac{max(\omega)}{2\pi}$

$\Rightarrow$ Sampling Rate $\geq 2 * \dfrac{\pi}{2\pi}$

$\Rightarrow$ Sampling Rate ≥ 1

This implies that a laminate signal L needs to be sampled at least once a second.

The precise quantity of these samples ($\mathcal{N}$) was then determined with another criterion: they must be able to describe a signals fundamental period [54]. While real signals may be aperiodic, the laminate signals are periodic due to their pure sinusoidal composition.

This periodicity-based criterion is motivated by how the Fast Fourier Transform (FFT) processes signals. Specifically, the FFT of $\mathcal{N}$ samples produces an output array of $\mathcal{N}$ frequency bins. Each bin represents a specific frequency and contains their corresponding amplitude. These bins are uniformly spaced between 0 (0° here) and the maximum detectable frequency (90° here).

Therefore, by sampling a period of the signal at the required rate, the number of bins will be spaced such that the desired frequency information are captured. For example, consider a laminate design with ply orientations $|\theta| \in 15°, 45°, 60°, 90°$. Their signal periodicity is determined by calculating the fundamental frequency:

Periodicity $= \dfrac{360}{\text{Fundamental Frequency}}$

$\Rightarrow$ Periodicity $= \dfrac{360}{\text{Greatest Common Divisor}(2 * [15°, 45°, 60°, 90°])}$

$\Rightarrow$ Periodicity $= \dfrac{360}{30}$

$\Rightarrow$ Periodicity $= 12$

Hence, the periodicity of the design case in this example is 12. So by using $\mathcal{N} = 13$ samples (from $T = 0$ to 12), the frequency bins generated by them correspond to [0°, 7.5°, 15°, 22.5°, 30°, 37.5°, 45°, 52.5°, 60°, 67.5°, 75°, 82.5°, 90°]. They contain the desired ply orientation information for this example case ($|\theta| \in [15°, 45°, 60°, 90°]$).

B.2. Derivation of exact signal patterns

For a given T, $a\ b$ and c can be solved by equating Eqs. (4) and (5):

$$\frac{1}{N}\sum_{k=1}^{N}[\cos 2\theta_k T] = a_T\left(L_1^A(T=0)\right) + b_T\left(L_1^A(T=1)\right) + c_T\left(L_1^A(T=2)\right)$$

$$\Rightarrow \frac{1}{N}\sum_{k=1}^{N}[\cos 2\theta_k T] = a_T\left(\frac{1}{N}\sum_{k=1}^{N}[\cos 2\theta_k \cdot 0]\right)$$
$$+ b_T\left(\frac{1}{N}\sum_{k=1}^{N}[\cos 2\theta_k \cdot 1]\right) + c_T\left(\frac{1}{N}\sum_{k=1}^{N}[\cos 2\theta_k \cdot 2]\right)$$

The summation rule adds the contribution of all N plies in the symmetric half of the FAD. For convenience, they are now replaced as a sum of p different ply orientations and their respective volume fractions v (the fraction of plies belonging to a certain orientation). For example, in a 20-layer FAD, if 5 plies have the orientation 45°, the volume fraction v of 45° is 0.25 ($\because$, 5/20=0.25).

$$\Rightarrow \begin{bmatrix} v_1 & v_2 & \cdots & v_p \end{bmatrix} \begin{bmatrix} \cos(2\theta_1 T) \\ \cos(2\theta_2 T) \\ \vdots \\ \cos(2\theta_p T) \end{bmatrix}$$

$$= a_T\left(\begin{bmatrix} v_1 & v_2 & \cdots & v_p \end{bmatrix} \begin{bmatrix} \cos(2\theta_1 \cdot 0) \\ \cos(2\theta_2 \cdot 0) \\ \vdots \\ \cos(2\theta_p \cdot 0) \end{bmatrix}\right)$$

$$+ b_T\left(\begin{bmatrix} v_1 & v_2 & \cdots & v_p \end{bmatrix} \begin{bmatrix} \cos(2\theta_1 \cdot 1) \\ \cos(2\theta_2 \cdot 1) \\ \vdots \\ \cos(2\theta_p \cdot 1) \end{bmatrix}\right)$$

$$+ c_T\left(\begin{bmatrix} v_1 & v_2 & \cdots & v_p \end{bmatrix} \begin{bmatrix} \cos(2\theta_1 \cdot 2) \\ \cos(2\theta_2 \cdot 2) \\ \vdots \\ \cos(2\theta_p \cdot 2) \end{bmatrix}\right)$$

$$\Rightarrow \begin{bmatrix} \cos(2\theta_1 T) \\ \cos(2\theta_2 T) \\ \vdots \\ \cos(2\theta_p T) \end{bmatrix} = a_T\left(\begin{bmatrix} \cos(2\theta_1 \cdot 0) \\ \cos(2\theta_2 \cdot 0) \\ \vdots \\ \cos(2\theta_p \cdot 0) \end{bmatrix}\right)$$
$$+ b_T\left(\begin{bmatrix} \cos(2\theta_1 \cdot 1) \\ \cos(2\theta_2 \cdot 1) \\ \vdots \\ \cos(2\theta_p \cdot 1) \end{bmatrix}\right)$$
$$+ c_T\left(\begin{bmatrix} \cos(2\theta_1 \cdot 2) \\ \cos(2\theta_2 \cdot 2) \\ \vdots \\ \cos(2\theta_p \cdot 2) \end{bmatrix}\right)$$

$$\Rightarrow \begin{bmatrix} \cos(2\theta_1 T) \\ \cos(2\theta_2 T) \\ \vdots \\ \cos(2\theta_p T) \end{bmatrix} = \begin{bmatrix} 1 & \cos(2\theta_1) & \cos(4\theta_1) \\ 1 & \cos(2\theta_2) & \cos(4\theta_2) \\ \vdots & \vdots & \vdots \\ 1 & \cos(2\theta_p) & \cos(4\theta_p) \end{bmatrix} \begin{bmatrix} a_T \\ b_T \\ c_T \end{bmatrix}$$

Table 11
Analytically-derived Signal Patterns for Laminates consisting [$\Delta15°$].

Orientations	$T = 0$	$T = 1$	$T = 2$	$T = 3$	$T = 4$	$T = 5$	$T = 6$
[0, 15, 30]	1	V_1^A	V_2^A	$6.46 - 10.19V_1^A + 4.73V_2^A$	$20.39 - 30.58V_1^A + 11.19V_2^A$	$35.32 - 51.98V_1^A + 17.66V_2^A$	$41.78 - 61.17V_1^A + 20.39V_2^A$
[0, 15, 45]	1	V_1^A	V_2^A	$3.73 - 6.46V_1^A + 3.73V_2^A$	$7.46 - 12.93V_1^A + 6.46V_2^A$	$7.46 - 13.93V_1^A + 7.46V_2^A$	$6.46 - 12.92V_1^A + 7.46V_2^A$
[0, 15, 60]	1	V_1^A	V_2^A	$1 - 2.73V_1^A + 2.73V_2^A$	$-2.73V_1^A + 3.73V_2^A$	$-3.73V_1^A + 4.73V_2^A$	$1 + 5.46(V_2^A - V_1^A)$
[0, 15, 75]	1	V_1^A	V_2^A	$-1 + 2V_2^A$	$-2 + V_2^A$	$-2 - V_1^A + 4V_2^A$	$-3 + 4V_2^A$
[0, 15, 90]	1	V_1^A	V_2^A	$-1.73 + V_1^A + 1.73V_2^A$	$-2 + V_2^A$	$-3.46 + V_1^A + 3.46V_2^A$	$-3 + 4V_2^A$
[0, 30, 45]	1	V_1^A	V_2^A	$3 - 5V_1^A + 3V_2^A$	$4 - 6V_1^A + 3V_2^A$	V_1^A	$-3 + 6V_1^A - 2V_2^A$
[0, 30, 60]	1	V_1^A	V_2^A	$1 - 2V_1^A + 2V_2^A$	V_2^A	V_1^A	1
[0, 30, 75]	1	V_1^A	V_2^A	$-0.46 + 0.19V_1^A + 1.26V_2^A$	$-0.39 + 0.58V_1^A + 0.8V_2^A$	$0.68 - 0.02V_1^A + 0.34V_2^A$	$0.21 + 1.17V_1^A - 0.39V_2^A$
[0, 30, 90]	1	V_1^A	V_2^A	$-1 + V_1^A + V_2^A$	V_2^A	V_1^A	1
[0, 45, 60]	1	V_1^A	V_2^A	$1 - V_1^A + V_2^A$	$2V_1^A - V_2^A$	V_1^A	$1 - 2V_1^A + 2V_2^A$
[0, 45, 75]	1	V_1^A	V_2^A	$0.26 + 0.46V_1^A + 0.26V_2^A$	$0.53 + 0.92V_1^A - 0.46V_2^A$	$0.53 - 0.07V_1^A + 0.53V_2^A$	$-0.46 + 0.92V_1^A + 0.53V_2^A$
[0, 45, 90]	1	V_1^A	V_2^A	V_1^A	1	V_1^A	V_2^A
[0, 60, 75]	1	V_1^A	V_2^A	$1 + 0.73V_1^A - 0.73V_2^A$	$0.73V_1^A + 0.26V_2^A$	$-0.26V_1^A + 1.26V_2^A$	$1 + 1.46V_1^A - 1.46V_2^A$
[0, 60, 90]	1	V_1^A	V_2^A	$1 + V_1^A - V_2^A$	V_2^A	V_1^A	1
[0, 75, 90]	1	V_1^A	V_2^A	$1.73 + V_1^A - 1.73V_2^A$	$-2 + V_2^A$	$3.46 + V_1^A - 3.46V_2^A$	$-3 + 4V_2^A$
[15, 30, 45]	1	V_1^A	V_2^A	$2.73 - 4.73V_1^A + 2.73V_2^A$	$2.73 - 4.73V_1^A + 1.73V_2^A$	$-2.73 + 3.73V_1^A - 2.73V_2^A$	$-6.46 + 9.46V_1^A - 5.46V_2^A$
[15, 30, 60]	1	V_1^A	V_2^A	$0.86 - 2V_1^A + 1.73V_2^A$	-0.5	$-0.86 + V_1^A - 1.73V_2^A$	$-2V_2^A$
[15, 30, 75]	1	V_1^A	V_2^A	$-0.5 + V_2^A$	-0.5	$0.5 - V_1^A - V_2^A$	$-2V_2^A$
[15, 30, 90]	1	V_1^A	V_2^A	$-1 + 0.73V_1^A + 0.73V_2^A$	$-0.73V_1^A + 0.26V_2^A$	$-0.26V_1^A - 1.26V_2^A$	$1 - 1.46V_1^A - 1.46V_2^A$
[15, 45, 60]	1	V_1^A	V_2^A	$0.73 - 1.26V_1^A + 0.73V_2^A$	$-0.73 + 1.26V_1^A - 1.73V_2^A$	$-0.73 + 0.26V_1^A - 0.73V_2^A$	$0.46 - 2.53V_1^A + 1.46V_2^A$
[15, 45, 75]	1	V_1^A	V_2^A	0	$-V_2^A$	$-V_1^A$	-1
[15, 45, 90]	1	V_1^A	V_2^A	$-0.26 + 0.46V_1^A - 0.26V_2^A$	$0.53 - 0.93V_1^A - 0.46V_2^A$	$-0.53 - 0.07V_1^A - 0.53V_2^A$	$-0.46 - 0.92V_1^A + 0.53V_2^A$
[15, 60, 75]	1	V_1^A	V_2^A	$0.5 - V_2^A$	-0.5	$0.5 - V_1^A + V_2^A$	$-2V_2^A$
[15, 60, 90]	1	V_1^A	V_2^A	$0.46 + 0.19V_1^A - 1.26V_2^A$	$-0.39 - 0.58V_1^A + 0.8V_2^A$	$-0.67 - 0.02V_1^A - 0.34V_2^A$	$0.21 - 1.17V_1^A - 0.39V_2^A$
[15, 75, 90]	1	V_1^A	V_2^A	$1 - 2V_2^A$	$-2 + V_2^A$	$2 - V_1^A - 4V_2^A$	$-3 + 4V_2^A$
[30, 45, 60]	1	V_1^A	V_2^A	$-2V_1^A$	$-2 + V_2^A$	V_1^A	$3 + 4V_2^A$
[30, 45, 75]	1	V_1^A	V_2^A	$-0.73 - 1.26V_1^A - 0.73V_2^A$	$-0.73 - 1.26V_1^A - 1.73V_2^A$	$0.73 + 0.26V_1^A + 0.73V_2^A$	$0.46 + 2.53V_1^A + 1.46V_2^A$
[30, 45, 90]	1	V_1^A	V_2^A	$-1 - V_1^A - V_2^A$	$-2V_1^A - V_2^A$	V_1^A	$1 + 2V_1^A + 2V_2^A$
[30, 60, 75]	1	V_1^A	V_2^A	$-0.86 - 2V_1^A - 1.73V_2^A$	-0.5	$0.86 + V_1^A + 1.73V_2^A$	$-2V_2^A$
[30, 60, 90]	1	V_1^A	V_2^A	$-1 - 2V_1^A - 2V_2^A$	V_2^A	V_1^A	1
[30, 75, 90]	1	V_1^A	V_2^A	$-1 - 2.73V_1^A - 2.73V_2^A$	$2.73V_1^A + 3.73V_2^A$	$-3.73V_1^A - 4.73V_2^A$	$1 + 5.46(V_2^A + V_1^A)$
[45, 60, 75]	1	V_1^A	V_2^A	$-2.73 - 4.73V_1^A - 2.73V_2^A$	$2.73 + 4.73V_1^A + 1.73V_2^A$	$2.73 + 3.73V_1^A + 2.73V_2^A$	$-6.46 - 9.46V_1^A - 5.46V_2^A$
[45, 60, 90]	1	V_1^A	V_2^A	$-3 - 5V_1^A - 3V_2^A$	$4 + 6V_1^A + 3V_2^A$	V_1^A	$-3 - 6V_1^A - 2V_2^A$
[45, 75, 90]	1	V_1^A	V_2^A	$-3.73 - 6.46V_1^A - 3.73V_2^A$	$7.46 + 12.92V_1^A + 6.46V_2^A$	$-7.46 - 13.93V_1^A - 7.46V_2^A$	$6.46 + 12.93V_1^A + 7.46V_2^A$
[60, 75, 90]	1	V_1^A	V_2^A	$-6.46 - 10.19V_1^A - 4.73V_2^A$	$20.39 + 30.58V_1^A + 11.19V_2^A$	$-35.32 - 51.98V_1^A - 17.66V_2^A$	$41.78 + 61.17V_1^A + 20.39V_2^A$

$$\Rightarrow \begin{bmatrix} a_T \\ b_T \\ c_T \end{bmatrix} = \begin{bmatrix} 1 & \cos(2\theta_1) & \cos(4\theta_1) \\ 1 & \cos(2\theta_2) & \cos(4\theta_2) \\ \vdots & \vdots & \vdots \\ 1 & \cos(2\theta_p) & \cos(4\theta_p) \end{bmatrix}^{-1} \begin{bmatrix} \cos(2\theta_1 T) \\ \cos(2\theta_2 T) \\ \vdots \\ \cos(2\theta_p T) \end{bmatrix}$$

To solve this system of equations, the dimensions across both ends should match. Hence, $p = 3$:

$$\Rightarrow \begin{bmatrix} a_T \\ b_T \\ c_T \end{bmatrix} = \begin{bmatrix} 1 & \cos(2\theta_1) & \cos(4\theta_1) \\ 1 & \cos(2\theta_2) & \cos(4\theta_2) \\ 1 & \cos(2\theta_3) & \cos(4\theta_3) \end{bmatrix}^{-1} \begin{bmatrix} \cos(2\theta_1 T) \\ \cos(2\theta_2 T) \\ \cos(2\theta_3 T) \end{bmatrix}$$

B.3. Complete list of signal patterns made for [$\Delta15°$] *laminates*

The analytically-derived and the manually-approximated signal patterns are presented in Tables 11 and 12 respectively.

B.4. Comparison of benchmark datasets

The original Bristol benchmarks [48] feature LP values that belong to SS with [$\Delta45°$] angles and ply counts of $N = [40, 80, 200]$. In order to have a more comprehensive assessment of a method's performance when designing SS with finer angle increments, new benchmarks were created using [$\Delta15°$] increments with a broader range of ply counts: $N = [10, 20, 40, 80, 100, 200]$. As shown in the 2D projections in Fig. 11, the new datasets cover a more diverse and extensive spread of LP values, all corresponding to real SS that satisfy design guidelines. Both datasets follow the same set of design guidelines, as stated in Table 10. The total number of test cases in all benchmark datasets can be summarised in Table 13.

Given that more stiffness combinations are possible with [$\Delta15°$] compared to [$\Delta45°$], the new benchmarks include many more test cases. An exception occurs for $N = 10$, as the number of guideline-compliant SS was limited. The laminates in these datasets were created

as follows. A uniform sample of V^A values was selected from the enumerated datasets of earlier (with $N = 5$ to 15). For each sample V^A, three corresponding V^D targets were chosen—one nearby, one at the median distance, and one farthest, from the original V^A. This ensured a varied and challenging set of test cases. The reference SS corresponding to these LPs were generated using the open-source GA pyTLO [41], with an exhaustive initial population and number of generations to ensure optimal convergence. This process ensured that all targets in the new benchmarks are realisable and well-distributed (at least in 2D projections).

B.5. Hyperparameters of all state-of-the-art methods seen in comparison studies

All methods were evaluated using hyperparameters recommended by their respective developers, ensuring fair and representative comparisons. Adjustments were made only when a method failed to produce feasible results with [$\Delta15°$] angles. For LAYLA [48], when the default repair parameters were insufficient for providing a guideline-compliant solution, the parameter controlling number of redesigned plies (n_{D1}) was incremented by 2 to enable feasible design. The full set of parameters are listed in Table 14.

For OptiBLESS [13], the parameters used in the work of Fedon et al. [48] are listed in Table 15. That work applied OptiBLESS to the bristol benchmark cases, and the same results are used in this study when comparing against LP2SS under identical conditions. However, due to limitations in OptiBLESS's population generation method, no hyperparameter setting was found that effectively designed feasible solutions for higher ply counts ($N=200$) and [$\Delta15°$] test cases, while satisfying all design guidelines. As a result, pyTLO [41] was employed for those cases, with its parameters detailed in Table 16. The GA
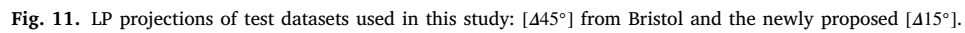
Fig. 11. LP projections of test datasets used in this study: [Δ45°] from Bristol and the newly proposed [Δ15°].

Table 12

Manually Approximated Signal Patterns for Laminates consisting [$\Delta15°$].

Approximate Pattern	$T = 0$	$T = 1$	$T = 2$	$T = 3$	$T = 4$	$T = 5$	$T = 6$
1	1	V_1^A	V_2^A	0	$-V_2^A$	$-V_1^A$	$-2V_2^A$
2	1	V_1^A	V_2^A	0	V_2^A	V_1^A	0
3	1	V_1^A	V_2^A	0	$1 - V_2^A$	$1 - V_1^A$	0
4	1	V_1^A	V_2^A	0	V_2^A	V_2^A	0
5	1	V_1^A	V_2^A	0	$2V_1^A$	V_1^A	0
6	1	V_1^A	V_2^A	$-V_2^A$	$V_1^A - V_2^A$	V_1^A	$-V_1^A$
7	1	V_1^A	V_2^A	$-V_2^A$	$V_2^A - V_1^A$	V_1^A	$-V_1^A$
8	1	V_1^A	V_2^A	V_1^A	V_2^A	V_1^A	$-V_1^A$
9	1	V_1^A	V_2^A	V_1^A	V_2^A	V_1^A	V_1^A
10	1	V_1^A	V_2^A	$0.5V_2^A$	$-V_2^A$	$-0.85V_2^A$	V_1^A
11	1	V_1^A	V_2^A	V_2^A	$0.5V_2^A$	$0.5(V_1^A + V_2^A)$	$0.5V_2^A$
12	1	V_1^A	V_2^A	$0.36(V_2^A - V_1^A)$	$0.34V_1^A$	V_1^A	$0.33V_1^A$
13	1	V_1^A	V_2^A	$1 + V_1^A - V_2^A$	V_2^A	V_1^A	1
14	1	V_1^A	V_2^A	$0.84V_1^A + 0.34V_2^A$	$0.59V_2^A$	$0.87V_1^A + 0.59V_2^A$	$0.43V_2^A$
15	1	V_1^A	V_2^A	$-2V_1^A$	$-0.5(V_1^A + V_2^A)$	V_1^A	$0.5(V_2^A - V_1^A)$
16	1	V_1^A	V_2^A	$0.36(V_2^A - V_1^A)$	$-0.34V_1^A$	$-V_1^A$	-0.6
17	1	V_1^A	V_2^A	$V_1^A + V_2^A$	$-V_1^A$	V_1^A	$-2V_1^A$
18	1	V_1^A	V_2^A	V_1^A	$0.5(V_1^A + V_2^A)$	V_1^A	$-0.5(V_1^A + V_2^A)$
19	1	V_1^A	V_2^A	$-2V_1^A$	$0.2V_2^A$	V_1^A	$-0.8V_2^A$
20	1	V_1^A	V_2^A	$-2V_1^A$	$5V_2^A$	V_1^A	$4V_2^A$
21	1	V_1^A	V_2^A	0	$1.66V_2^A$	$-V_1^A$	0
22	1	V_1^A	V_2^A	$V_2^A - 0.5$	-0.5	$0.5 - (V_1^A + V_2^A)$	$-2V_2^A$
23	1	V_1^A	V_2^A	$0.34V_2^A + 0.84V_1^A$	$0.594V_2^A$	$0.594V_2^A + 0.87V_1^A$	$0.4375V_2^A$
24	1	V_1^A	V_2^A	$-2V_1^A$	$0.2V_2^A$	V_1^A	$-0.8V_2^A$
25	1	V_1^A	V_2^A	$-2V_1^A$	$5V_2^A$	V_1^A	$4V_2^A$
26	1	V_1^A	V_2^A	$-\dfrac{V_1^A}{2.3333}$	$1.00669(V_1^A - V_2^A)$	$\dfrac{V_2^A}{2.3333} - V_1^A$	$-2V_2^A$
27	1	V_1^A	V_2^A	$0.3661V_1^A$	$-2V_2^A$	$-0.268V_1^A$	$-2V_2^A$
28	1	V_1^A	V_2^A	$2V_2^A$	0	$V_2^A - V_1^A$	V_2^A
29	1	V_1^A	V_2^A	$0.5V_2^A$	0	$V_2^A - V_1^A$	$-2V_2^A$
30	1	V_1^A	V_2^A	$-V_2^A$	0	$V_2^A - V_1^A$	V_2^A
31	1	V_1^A	V_2^A	V_1^A	V_2^A	V_1^A	$\dfrac{V_2^A}{3}$

Table 13

Total number of test cases for different ply counts and [$\Delta\theta$] across benchmark datasets.

N	Bristol Benchmarks [$\Delta45°$] [48]	New Benchmarks [$\Delta15°$] [55]
10	–	68
20	–	450
40	200	450
80	200	450
100	–	450
200	200	450

Table 14

LAYLA Hyperparameters [48].

Maximum Outer loops	5
Branching limit of beam search	50
Fitness limit	1E−10
No. of iterations	1
Objective Function	Mean Squared Error
No. of redesigned plies n_{D1}	6 (+2)
No. of ply-shifts tested n_{D2}	10
No. of repetitions of ply-shift algorithm n_{D3}	2

Table 15

OptiBLESS Hyperparameters [13,48].

Maximum generations	100
Population Size	200
Elitism %	1
Crossover %	75
Fitness limit	1E−10
No. of iterations	5
Objective Function	Root Mean Squared Error
Feasibility penalty factor	100

Table 16

pyTLO Hyperparameters [41].

Maximum generations	1000
Population Size	100
Elitism %	5
Crossover %	75
Mutation %	25
Fitness limit	1E−4
Feasibility penalty factor	100
No. of iterations	1
Objective Function	Root Mean Squared Error

Table 17

DMRG Hyperparameters [38].

No. of Sweeps	40
Maximum Bond Dimension	8
Sweep Sequence	L
Objective Function	Root Mean Squared Error
No. of Iterations	5
Disorientation Penalty	1/N
Contiguity Penalty	0.5/N
Balance Penalty	0.2/N

implementation of pyTLO was robust enough to converge to similar results when re-run multiple times. Hence, they were not re-run multiple times, like OptiBLESS and other nondeterministic methods require.

For DMRG [38], the hyperparameter settings were adopted directly from the developer's publication, as shown in Table 17. Given the nondeterministic nature, the tool was re-run for multiple iterations to match the same solution quality as the developer. As the current state of DMRG is tuned primarily for [$\Delta45°$] angles, they were unable to be used to yield feasible results with [$\Delta15°$].

B.6. Empirical time complexity of tested SS design methods

The time taken to design an N-layer SS was empirically determined for each method using polynomial regression of results from the

Table 18
Empirical time complexity of LP2SS and other SS design methods, as a function of ply count N and allowable angle set.

	[$\Delta45°$]	[$\Delta15°$]
LP2SS	$t = 0.00127N + 0.01366$	$t = -(9.71723E-06)N^2 + (5.20035E-03)N + 0.12097$
BB	$t = 0.32730N - 2.97030$	$t = (1.47236E-03)N^2 + 0.66927N - 4.54268$
MILP	$t = 0.35954N - 9.04419$	–
GA	$t = 1.21673N + 102.57415$	$t = (5.62316E-03)N^2 + 0.61318N + 46.51798$

comparison studies (in Section 5). The resulting equations approximate time complexity as a function of the number of layers (N) and the angle set used ([$\Delta45°$] or [$\Delta15°$]), and are summarised in Table 18.

These regressions reflect the average behaviour observed during testing. The Branch & Bound (BB) results are based on LAYLA [48]. Mixed Integer Linear Programming (MILP) results are based on the Quantum-inspired DMRG method [38]. For Genetic Algorithm (GA), OptiBLESS [13] was used for cases involving [$\Delta45°$], while pyTLO [41] for [$\Delta15°$]. Estimates for MILP are not provided for [$\Delta15°$], as the current state of DMRG can reliably produce results only for [$\Delta45°$].

References

[1] BP statistical review of world energy 2023. 2023.
[2] Airbus. A350 Less Operating Cost. More Capabilities, URL https://aircraft.airbus.com/en/aircraft/a350-clean-sheet-clean-start/a350-less-operating-cost-more-capabilities.
[3] Griffiths B. Boeing sets pace for composite usage in large civil aircraft. Composites World; 2005.
[4] Hyer M, Lee H. The use of curvilinear fiber format to improve buckling resistance of composite plates with central circular holes. Compos Struct 1991;18(3):239–61. http://dx.doi.org/10.1016/0263-8223(91)90035-W.
[5] Peeters DMJ. Design optimisation of practical variable stiffness and thickness laminates. Delft University of Technology; 2017.
[6] Ghiasi H, Pasini D, Lessard L. Optimum stacking sequence design of composite materials Part I: Constant stiffness design. Compos Struct 2009;90(1):1–11. http://dx.doi.org/10.1016/j.compstruct.2009.01.006.
[7] Tauchert T, Adibhatla S. Design of laminated plates for maximum stiffness. J Compos Mater 1984;18(1):58–69. http://dx.doi.org/10.1177/002199838401800105.
[8] Olmedo R, Gürdal Z. Buckling response of laminates with spatially varying fiber orientations. In: 34th structures, structural dynamics and materials conference. American Institute of Aeronautics and Astronautics; 1993, http://dx.doi.org/10.2514/6.1993-1567.
[9] IJsselmuiden S. Optimal design of variable stiffness composite structures using lamination parameters. 2011, URL http://resolver.tudelft.nl/uuid:973a564b-5734-42c4-a67c-1044f1e25f1c.
[10] Gürdal Z, Haftka RT, Hajela P. Design and optimization of laminated composite materials. Wiley; 1999.
[11] Bailie JA, Ley RP, Pasricha A. A summary and review of composite laminate design guidelines. Tech. rep., Northrop Grumman; 1997.
[12] Kassapoglou C. Design and analysis of composite structures: With applications to aerospace structures. 1st ed. Wiley; 2013, .
[13] Macquart T. OptiBLESS (Optimisation of BLEnded stacking sequence) toolbox. 2015, URL https://github.com/TMacquart/OptiBLESS.
[14] Fedon N. Stacking-sequence design of composite laminates with many plies. University of Bristol; 2021.
[15] Tsai SW. AD. 668 761 invariant properties of composite materials, Derivation for LPs.
[16] Balabanov V, Weckner O, Epton M, Mabson G, Cregger S, Blom A. Optimal design of a composite sandwich structure using lamination parameters. American Institute of Aeronautics and Astronautics; 2012, http://dx.doi.org/10.2514/6.2012-1520.
[17] Grenestedt J, Gudmundson P. Layup Optimization of Composite Material Structures. In: Optimal design with advanced materials. Elsevier; 1993, p. 311–36.
[18] Beckwith S. Designing with composites: Suggested "best practices" rules. SAMPE J 2009;45:36–7.
[19] Peeters DM, Abdalla MM. Design guidelines in nonconventional composite laminate optimization. In: American institute of aeronautics and astronautics, J Aircr In: American institute of aeronautics and astronautics, 2017;54(4):1454–64.http://dx.doi.org/10.2514/1.C034087,
[20] York CB. Unified approach to the characterization of coupled composite laminates: Benchmark configurations and special cases. J Aerospace Eng 2010;23(4):219–42. http://dx.doi.org/10.1061/(ASCE)AS.1943-5525.0000036.
[21] Montemurro M, Izzi MI, El-Yagoubi J, Fanteria D. Least-weight composite plates with unconventional stacking sequences: Design, analysis and experiments. J Compos Mater 2019;53(16):2209–27. http://dx.doi.org/10.1177/0021998318824783.
[22] Abdalla MM, Gürdal Z, Kassapoglu C. Formulation of composite laminate robustness constraint in lamination parameters space. In: 50th AIAA/ASME/ASCE/AHS/ASC structures, structural dynamics, and materials conference. Structures, structural dynamics, and materials and co-located conferences, American Institute of Aeronautics and Astronautics; 2009, http://dx.doi.org/10.2514/6.2009-2478.
[23] Albazzan MA, Harik R, Tatting B, Gurdal Z. Efficient design optimization of nonconventional laminated composites using lamination parameters: A state of the art. Compos Struct 2019;209:362–74. http://dx.doi.org/10.1016/j.compstruct.2018.10.095.
[24] Miki M. Material design of composite laminates with required in-plane elastic properties. Prog Sci Eng Compos 1982.
[25] Hammer VB, Bendsøe MP, Lipton R, Pedersen P. Parametrization in laminate design for optimal compliance. Int J Solids Struct 1997;34(4):415–34. http://dx.doi.org/10.1016/S0020-7683(96)00023-6.
[26] Autio M. Optimization of coupled thermal-structural problems of laminated plates with lamination parameters. Struct Multidiscip Optim 2001;21(1):40–51. http://dx.doi.org/10.1007/s001580050166, .
[27] Diaconu CG, Sekine H. Layup optimization for buckling of laminated composite shells with restricted layer angles. AIAA J 2004;42(10):2153–63. http://dx.doi.org/10.2514/1.931, .
[28] van Campen JMJF, Gürdal Z. Retrieving variable stiffness laminates from lamination parameters distribution. In: 50th AIAA/ASME/ASCE/AHS/ASC structures, structural dynamics, and materials conference. American Institute of Aeronautics and Astronautics; 2009, http://dx.doi.org/10.2514/6.2009-2183.
[29] Viquerat AD. A continuation-based method for finding laminated composite stacking sequences. Compos Struct 2020;238. http://dx.doi.org/10.1016/j.compstruct.2020.111872.
[30] Grediac M. A procedure for designing laminated plates with required stiffness properties. Application to thin quasi-isotropic quasi-homogeneous uncoupled laminates. J Compos Mater 1999;33(20):1939–56. http://dx.doi.org/10.1177/002199839903302005.
[31] Grediac M. On the stiffness design of thin woven composites. Compos Struct 2001;51(3):245–55. http://dx.doi.org/10.1016/S0263-8223(00)00135-5.
[32] Peeters DM, Hong Z, Abdalla MM. A compliance approximation method applied to variable stiffness composite optimisation. Struct Multidiscip Optim 2018;58(5):1981–2001. http://dx.doi.org/10.1007/s00158-018-2007-2.
[33] Bangera SS, Castro SG. Deflation constraints for global optimization of composite structures. Compos Struct 2025;357:118916. http://dx.doi.org/10.1016/j.compstruct.2025.118916.
[34] Haftka RT, Walsh JL. Stacking-sequence optimization for buckling of laminated plates by integer programming. AIAA J 1992;30(3):814–9. http://dx.doi.org/10.2514/3.10989, URL https://arc.aiaa.org/doi/10.2514/3.10989.
[35] Liu D, Toropov V. A lamination parameter-based strategy for solving an integer-continuous problem arising in composite optimization. Comput Struct 2013;128:170–4. http://dx.doi.org/10.1016/j.compstruc.2013.06.003.
[36] Ntourmas G, Ozcan E, Chronopoulos D, Glock F, Daoud F. Towards a streamlined stacking sequence optimisation methodology for blended composite aircraft structures. In: Proceedings of the 8th European conference for aeronautics and space sciences. 2019, http://dx.doi.org/10.13009/EUCASS2019-632,
[37] Wulff A, Chen B, Steinberg M, Tang Y, Möller M, Feld S. Quantum computing and tensor networks for laminate design: A novel approach to stacking sequence retrieval. Comput Methods Appl Mech Engrg 2024;432:117380. http://dx.doi.org/10.1016/j.cma.2024.117380.
[38] Wulff A, Venkata SM, Chen B, Feld S, Möller M, Tang Y. Quantum-assisted stacking sequence retrieval and laminated composite design. 2024, http://dx.doi.org/10.48550/arXiv.2411.10303.
[39] Cortez P. Population based search. In: Modern optimization with r. Springer International Publishing; 2021, p. 89–151, URL https://link.springer.com/10.1007/978-3-030-72819-9_5.
[40] van Campen JMJF, Seresta O, Abdalla MM, Gürdal Z. General blending definitions for stacking sequence design of composite laminate structures. In: 49th AIAA/ASME/ASCE/AHS/ASC structures, structural dynamics, and materials conference. American Institute of Aeronautics and Astronautics; 2008, http://dx.doi.org/10.2514/6.2008-1798.

[41] Sousa Vicente F. Stacking sequence retrieval of large composite structures in bi-step optimization strategies using mechanical constraints. 2019, URL http://resolver.tudelft.nl/uuid:0d8644c9-099d-404c-890f-9242541414b5.

[42] Narita Y. Layerwise optimization for the maximum fundamental frequency of laminated composite plates. J Sound Vib 2003;263(5):1005–16. http://dx.doi.org/10.1016/S0022-460X(03)00270-0.

[43] Narita Y, Hodgkinson J. Layerwise optimisation for maximising the fundamental frequencies of point-supported rectangular laminated composite plates. Compos Struct 2005;69(2):127–35. http://dx.doi.org/10.1016/j.compstruct.2004.05.021.

[44] Terada Y, Todoriki A, Shimamura Y. Stacking sequence optimizations using fractal branch and bound method for laminated composites. 2001, https://doi-org.tudelft.idm.oclc.org/10.1299/jsmea.44.490.

[45] Todoroki A, Terada Y. Improved fractal branch and bound method for stacking-sequence optimizations of laminates. AIAA J 2004;42(1):141–8. http://dx.doi.org/10.2514/1.9038.

[46] Matsuzaki R, Todoroki A. Stacking-sequence optimization using fractal branch-and-bound method for unsymmetrical laminates. Compos Struct 2007;78(4):537–50. http://dx.doi.org/10.1016/j.compstruct.2005.11.015.

[47] Liu X, Featherston C, Kennedy D. Two-level layup optimization of composite laminate using lamination parameters. Compos Struct 2019;211:337–50. http://dx.doi.org/10.1016/j.compstruct.2018.12.054.

[48] Fedon N, Weaver P, Pirrera A, Macquart T. A method using beam search to design the lay-ups of composite laminates with many plies. Compos C Open Access 2021;4. http://dx.doi.org/10.1016/j.jcomc.2020.100072.

[49] Fedon N, Weaver PM, Pirrera A, Macquart T. A repair algorithm for composite laminates to satisfy lay-up design guidelines. Compos Struct 2021;259:113448. http://dx.doi.org/10.1016/j.compstruct.2020.113448.

[50] Adler EJ, Martins JRRA. Efficient aerostructural wing optimization considering mission analysis. J Aircr 2023;60(3):800–16. http://dx.doi.org/10.2514/1.C037096, .

[51] Dähne S, Werthen E, Zerbst D, Tönjes L, Traub H, Hühne C. Lightworks, a scientific research framework for the design of stiffened composite-panel structures using gradient-based optimization. Struct Multidiscip Optim 2024;67(5):70. http://dx.doi.org/10.1007/s00158-024-03783-1.

[52] Manikandan R, Dähne S. LP2SS: Efficient conversion of lamination parameters into stacking sequences using fast Fourier transforms and branch & bound (code). 2025, Github, URL https://github.com/DLR-SY/lp2ss.

[53] Knopp K. Theory of functions. Dover books on mathematics, Dover ed. Dover Publications; 1996.

[54] Smith SW. Digital signal processing: A practical guide for engineers and scientists. 3rd ed. Elsevier Science & Technology; 2013.

[55] Manikandan R, Dähne S. LP2SS: Efficient conversion of lamination parameters into stacking sequences using fast Fourier transforms and branch & bound (datasets). 2025, http://dx.doi.org/10.5281/zenodo.17078849, Zenodo.

[56] Macquart T, Werter N, De Breuker R. Aeroelastic design of blended composite structures using lamination parameters. J Aircr 2017;54(2):561–71. http://dx.doi.org/10.2514/1.C033859.

[57] Bordogna MT, Lancelot P, Bettebghor D, De Breuker R. Static and dynamic aeroelastic tailoring with composite blending and manoeuvre load alleviation. Struct Multidiscip Optim 2020;61(5):2193–216. http://dx.doi.org/10.1007/s00158-019-02446-w.

[58] Williams FW, Kennedy D, Butler R, Anderson MS. VICONOPT - program for exact vibration and buckling analysis or design of prismatic plate assemblies. AIAA J 1991;29(11):1927–8.

[59] Tsai S. Double–double: New family of composite laminates. AIAA J 2021;59(11):4293–305. http://dx.doi.org/10.2514/1.J060659.

[60] Zerbst D, Tönjes L, Dähne S, Werthen E, Kappel E, Hühne C. Equivalent plate formulation of Double–Double laminates for the gradient-based design optimization of composite structures. Compos Struct 2025;354:118786. http://dx.doi.org/10.1016/j.compstruct.2024.118786.

[61] Grihon S, Krog L, Bassir D. Numerical Optimization applied to structure sizing at AIRBUS: A multi-step process. Int J Simul Multidiscip Des Optim 2009;3(4):432–42. http://dx.doi.org/10.1051/ijsmdo/2009020.

[62] Zein S, Colson B, Grihon S. A primal-dual backtracking optimization method for blended composite structures. Struct Multidiscip Optim 2012;45(5):669–80. http://dx.doi.org/10.1007/s00158-011-0716-x.

[63] Setoodeh S. Optimal design of variable-stiffness fiber-reinforced composites using cellular automata. 2005, URL http://resolver.tudelft.nl/uuid:89b628b0-a91a-4d32-b5dc-598b11d327cf.

[64] Wu Z, Raju G, Weaver P. Framework for the buckling optimization of variable-angle tow composite plates. AIAA J 2015-12;53(12):3788–804. http://dx.doi.org/10.2514/1.J054029.

[65] Werthen E, Dähne S. Design- and manufacturing constraints witin the gradient based optimization of a composite aircraft wingbox. In: 6th airframe structural design conference. 2018.

[66] Vannucci P, Vincenti A. The design of laminates with given thermal/hygral expansion coefficients: A general approach based upon the polar-genetic method. Compos Struct 2007;79(3):454–66. http://dx.doi.org/10.1016/j.compstruct.2006.02.004.